Measurement and analysis of the infraredactive stretching fundamental (v3) of UF6

Jack P. Aldridge, Ernest G. Brock, Henry Filip, Herbert Flicker, Kenneth Fox et al.

Citation: J. Chem. Phys. **83**, 34 (1985); doi: 10.1063/1.449777
View online: http://dx.doi.org/10.1063/1.449777
View Table of Contents: http://jcp.aip.org/resource/1/JCPSA6/v83/i1
Published by the American Institute of Physics.

Measurement and analysis of the infrared-active stretching fundamental (ν_3) of UF_6[a)]

Jack P. Aldridge, Ernest G. Brock, Henry Filip, and Herbert Flicker
University of California, Los Alamos National Laboratory, Los Alamos, New Mexico 87545

Kenneth Fox
Department of Physics and Astronomy, University of Tennessee, Knoxville, Tennessee 37996–1200

Harold W. Galbraith, Redus F. Holland, K. C. Kim, and Burton J. Krohn[b)]
University of California, Los Alamos National Laboratory, Los Alamos, New Mexico 87545

Dale W. Magnuson
Union Carbide Corporation, Oak Ridge Gaseous Diffusion Plant, Oak Ridge, Tennessee 37830

William B. Maier II, Robin S. McDowell,[b)] and Chris W. Patterson
University of California, Los Alamos National Laboratory, Los Alamos, New Mexico 87545

Willis B. Person
Department of Chemistry, University of Florida, Gainesville, Florida 32611

D. F. Smith and George K. Werner
Union Carbide Corporation, Oak Ridge Gaseous Diffusion Plant, Oak Ridge, Tennessee 37830

(Received 4 February 1985; accepted 21 March 1985)

High-resolution spectra of the infrared-active stretching fundamental ν_3 of $^{238}UF_6$ have been obtained between 620.6 and 633.5 cm^{-1} using tunable semiconductor diode lasers. Interference from hot bands was suppressed by cooling the UF_6 in a supersonic expansion, and useful monomer concentrations were produced with effective temperatures of < 100 K. Portions of the band from $P(77)$ to $R(66)$ are illustrated. All transitions from the vibrational ground state have been assigned, and the Q branch has been fully analyzed. A total of 43 line frequencies and 110 frequency differences extending in J to $P(77)$, $Q(91)$, and $R(67)$ has been used to fit seven spectroscopic constants. The ground- and excited-state values of the rotational constant B could be individually determined, and the U–F bond length in the ground vibrational state is $r_0 = 1.9962 \pm 0.0007$ Å. The Q branch of $^{235}UF_6$ has also been analyzed and the $^{235}UF_6$–$^{238}UF_6$ ν_3 isotope shift measured to be $0.603\ 79 \pm 0.000\ 17$ cm^{-1}. The isotope shift and the Coriolis constant ζ_3 have been used to refine the general quadratic intramolecular force field of UF_6, and the Cartesian displacement coordinates of both infrared-active fundamentals are illustrated and compared with those of SF_6.

INTRODUCTION

Recently much attention has been given to possible photochemical schemes of uranium isotope separation to replace or supplement conventional gaseous diffusion and gas centrifuge technologies.[1–3] Almost all molecular photochemical approaches have concentrated on UF_6: it is the only uranium-containing compound having significant volatility, its industrial production and handling are well developed, and only modest photolysis energy is needed to affect its dissociation or reaction. Most of these approaches involve pumping an infrared absorption feature of UF_6, either alone or in combination with another pumping frequency, to promote photolysis, chemical reaction, multiphoton absorption, and/or dissociation. While some work has been reported using 10 μm CO_2 lasers as the sole pump source,[4] UF_6 absorbs only weakly in this region, and most investigations have focused on the ν_3 stretching mode at 628 cm^{-1} for at least the first pumping step. This is the strongest infrared-active vibrational fundamental, and it exhibits the largest isotope shift of about 0.6 cm^{-1}. Since photodissociation of UF_6 at 16 μm was first reported in 1978,[5,6] there has been a great deal of further work at several laboratories, for which we cite only a few summary and review papers.[1,7–11] Recently, successful isotope separation of UF_6 has been reported in which ν_3 was pumped with radiation from H_2 Raman lasers[12] and CF_4 lasers.[13] In understanding these experiments, details of the infrared spectrum of UF_6, and of the ν_3 band in particular, are obviously of the greatest importance.

Vibrational spectroscopy of UF_6 as it stood a decade ago was summarized by McDowell, Asprey, and Paine,[14] who studied the infrared and Raman spectra of 44 fundamental and combination bands of UF_6 vapor at spectral resolutions of the order of 1 cm^{-1}. They reported the general quadratic force constants determined from isotope shifts and Coriolis constants, but the latter quantities had to be estimated from unresolved band contours, for no detailed rotational structure was observed at the grating resolution available then.

Since 1974 some further spectroscopy of UF_6 using "conventional" infrared techniques has been reported. The

[a)] Work performed under the auspices of the United States Department of Energy.

[b)] Authors to whom correspondence should be addressed.

 0021-9606/85/130034-15$02.10

vapor spectrum has been reexamined with a Fourier transform infrared (FTIR) spectrometer and the frequency dependence of the small-signal isotopic selectivity for ν_3 and for the binary combination bands was reported.[15] Absorption of weak UF_6 ternary combinations that overlap CO_2 laser lines between 925 and 1044 cm^{-1} has been measured.[16] There have also been several condensed-phase infrared studies of UF_6 in rare-gas,[17] CO,[17] and SiH_4[18,19] matrices and in cryogenic solutions[20,21]; the matrix work also included studies of the laser-induced photolytic decomposition or reaction of UF_6.

Raman spectroscopy of UF_6 vapor has been reported in greater detail by the use of CARS techniques,[22–24] although individual rotational lines have yet to be resolved. The absolute Raman scattering cross section of ν_1 has been determined and used for density measurements of UF_6 vapor.[25] Matrix Raman spectra have been reported,[17] and Bernstein and Meredith[26] have discussed in detail the UF_6 vibrational and excitonic band structure inferred from their Raman studies of neat and mixed crystals.

A significant advance in the rovibrational spectroscopy of UF_6 vapor requires a great improvement in resolution over that available from grating or FTIR instruments. Because of the large UF_6 vibrational partition function ($Z_v = 242$ at 300 K), however, resolution *per se* is hardly sufficient: 99.6% of UF_6 molecules are in excited vibrational states at 300 K, so the spectrum consists of the superposition of many hundreds of hot bands, resulting in a dense, chaotic, and quasicontinuous fine structure. Further, in each of these bands the rotational structure is widely spread, since the most populated rotational state is $J = 63$ at 300 K.[27] These difficulties can be reduced by cooling, but the vapor pressure of UF_6 (about 127 Torr at 300 K; 1 Torr at 243 K where $Z_v = 65$)[28] limits the degree with which this can be accomplished without resorting to special techniques.

The new experimental approach that is required has been met with tunable semiconductor diode lasers that can achieve Doppler-limited spectral resolution even for a relatively heavy molecule such as UF_6, and supersonic adiabatic expansion through nozzles to obtain useful number densities of gaseous UF_6 molecules supercooled to temperatures below 100 K. Such work has been in progress in several laboratories since about 1971,[2] though most of it remains unpublished or has appeared only in a very preliminary form.[1–3,29–32] Some diode laser work has also been done with statically cooled UF_6, using path lengths of up to 400 m to overcome low vapor pressures ($p \approx 3 \times 10^{-6}$ Torr at $T = 165$ K). This includes studies of the integrated band strength and line strengths in ν_3,[33] and of the hot bands accompanying ν_3.[34] Recently Takami *et al.*[35] reported diode laser spectra of supersonically cooled UF_6. They measured 154 lines of ν_3 from $P(21)$ to $R(27)$, fitted the spectroscopic constants, and determined the $^{235}UF_6$–$^{238}UF_6$ isotope shift. This is the first detailed high-resolution spectroscopy of UF_6 to appear in print, but it included no Q-branch analysis and was limited to relatively low values of the total angular momentum quantum number J.

In the present paper we report some of the high-resolution spectroscopy of flow-cooled UF_6 that was carried out at Los Alamos and Oak Ridge from 1973 to 1982. Much of this effort was spent in first developing experimental techniques for the high-resolution infrared spectroscopy of flow-cooled molecules, and methods for analyzing the complex spectra of heavy spherical tops. These techniques have since become familiar through their application to other molecules, but they were first developed for and applied to the problem of UF_6 spectroscopy. We will discuss here the vibration-rotation analysis of ν_3 and the use of this information to refine the general quadratic force field of UF_6. Other aspects of the spectroscopy and photophysics of this molecule, particularly the high-resolution analysis of combination and overtone bands and studies of the $n\nu_3$ absorption ladder, will be reported elsewhere.

EXPERIMENTAL

The experimental work summarized here was carried out over the course of a decade at two different laboratories. We have selected a representative sample of data from this large and diverse store of information. Portions of the P, Q, and R branches are illustrated in Figs. 1–9, in order of increasing wave number. While some spectra were obtained by static cooling down to 165 K, the most useful data consist of spectra of UF_6 flow-cooled to temperatures of 90 K or lower, at which at least 55% of the molecules are in the ground vibrational state and the most-populated rotational state is $J \leqslant 34$. The importance of this technique justifies a brief discussion of the principles involved.

When a gas is allowed to expand isentropically in a diverging nozzle, random thermal energy is converted into directed kinetic energy of mass flow, and the gas is cooled. For ideal nozzles and perfect gases, the ratio of the temperature

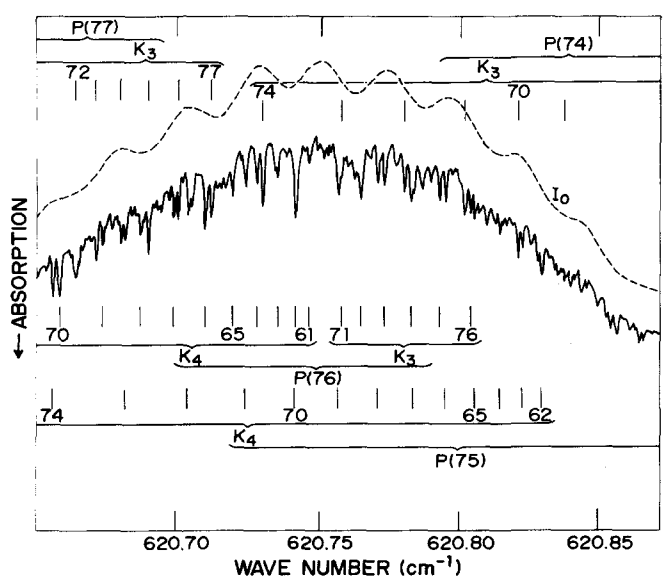

FIG. 1. Absorption spectrum of flow-cooled $^{238}UF_6$ in the $P(74)$ to $P(77)$ region. The K_3 and K_4 notation for identifying the clustered lines is discussed in the text. The continuum absorption above the background (I_0) is probably caused by scattering and absorption due to UF_6 polymers and/or to unresolved hot bands. Flow conditions: the gas mixture was 1.3% UF_6 in Ar (depleted UF_6 containing 0.2% ^{235}U); temperature and number density unknown; optical path 20 cm.

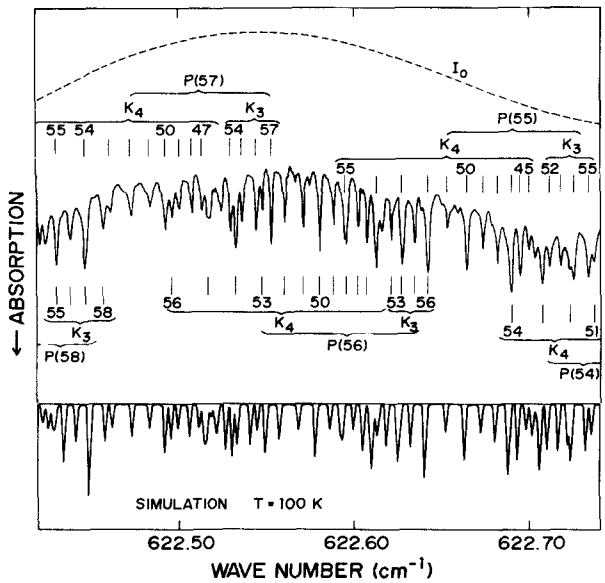

FIG. 2. The $P(54)$ to $P(58)$ region as observed, and as simulated using the spectroscopic constants of Table V and a linewidth of 0.0016 cm^{-1} (FWHM). The simulation reproduces the experimental spectrum quite satisfactorily, despite a slight nonlinearity in the wave number scale of the latter at the low-frequency end of the scan. Experimental conditions as for Fig. 1.

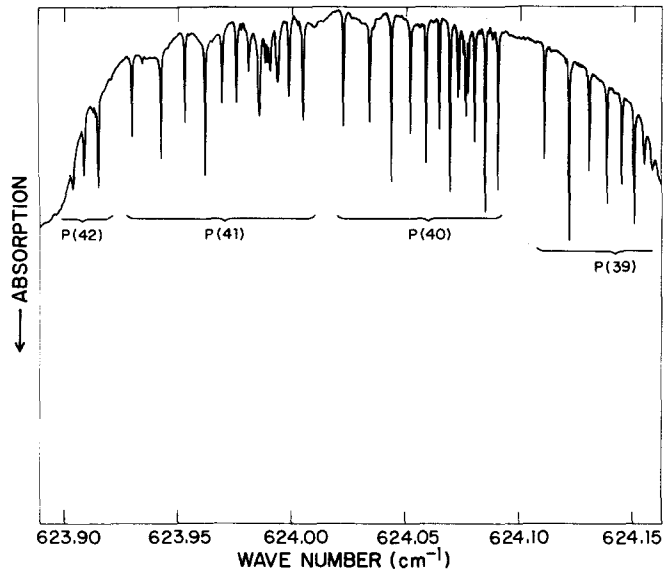

FIG. 3. The $P(39)$ to $P(42)$ region; experimental conditions as for Fig. 1. Note that the diode performance deteriorates at both ends of the scan.

T of the expanding gas to the gas temperature T_0 before expansion is [36,37]

$$T/T_0 = (p/p_0)^{(\gamma-1)/\gamma} = (\rho/\rho_0)^{\gamma-1},$$

where p and ρ are the gas pressure and density, respectively, and $\gamma = C_p/C_v$ is the ratio of heat capacity at constant pressure to that at constant volume. Obviously the temperature T achieved under given conditions decreases as γ increases. For monatomic and light diatomic gases, $\gamma = 1.67$ and 1.40, respectively; for UF_6 $\gamma \approx 1.07$ at 300 K,[28] increasing somewhat at lower temperatures. For such heavy polyatomic molecules, cooling can be better effected by expanding a light carrier gas that has been seeded with a small fraction of the heavier molecule, which will be cooled to the translational temperature of the carrier gas by collisions with molecules of the latter. The rotational and vibrational temperatures of the seed molecules may or may not reach this value, depending upon the relative relaxation rates. In the nozzles employed in the present work, equilibration between translational, rotational, and vibrational temperatures was generally complete. However, phase equilibration under these conditions is very slow, and most of the seed molecules persist as gas-phase monomers despite very high supersaturation ratios. When condensation occurs,[32] it will appear in the infrared spectrum as a featureless continuum absorption (cf. Figs. 1, 2, and 8); this may be important in studying the kinetics of the expansion, but it will have no effect on the sharp absorption features associated with the supercooled monomers.

Several different nozzles were used at Los Alamos and Oak Ridge. These had significantly different operating characteristics, though the differences are of little consequence in terms of the spectra obtained. Los Alamos employed two-dimensional contoured nozzles with a slit throat,[1,2] similar

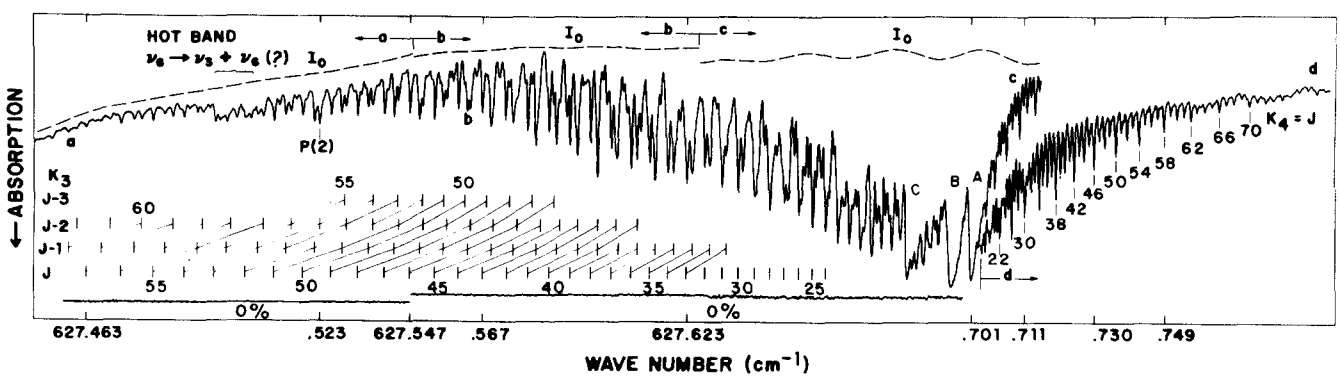

FIG. 4. The Q branch of $^{238}UF_6$. This figure is a composite of four different scans, (a) to (d). Experimental conditions were generally as for Fig. 1, but differed slightly between scans; T was less than 90 K for all scans. Some of the spectral features are identified. Features assigned to the same $Q(J)$ manifold but corresponding to different angular momenta, K_3, about a threefold axis of molecular symmetry, are connected by diagonal lines at the left of the figure. To the right, the components of $Q_A(J)$, for which $K_4 = J$, are labeled. A, B, and C designate the three subbandheads. The band origin occurs near the peak of the A subbandhead (actually about 0.0004 cm^{-1} to the blue).

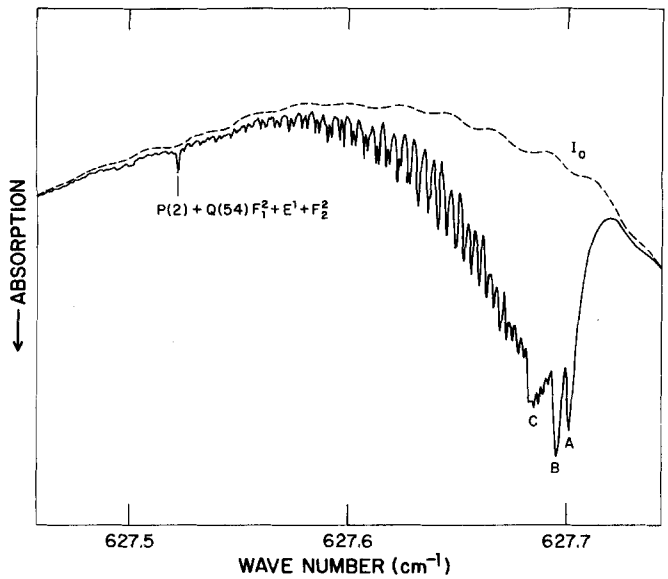

FIG. 5. The Q branch of flow-cooled $^{238}UF_6$ at approximately $T = 40$ K. At this lower temperature $P(2)$ is more prominent than in Fig. 4. On the high-frequency side of the Q branch ($\nu > 627.7$ cm^{-1}) the diode performance is degraded and the structure shown in Fig. 4 is not resolved.

to the configurations used in the first gas dynamic lasers. In these, the expansion proceeds rapidly near the throat and a uniform parallel supersonic flow forms in the central core for a distance of several centimeters downstream. These nozzles were operated in a pulsed mode in a recirculating loop system, in which the diode was scanned in synchronization with the pulse frequency; and also in a "blow-down" mode in which the gas was allowed to expand into a large evacuated tank, thus providing several seconds of continuous operation in which to record data. Flow conditions were typically in the following ranges: mole fraction of UF_6 in the carrier gas (Ar or N_2) 0.001–0.01, $p_0 = 300$–500 Torr, $T_0 = 300$ K, $p = 5$–10 Torr, and $T = 60$–110 K.

Most of the spectra reported here were obtained at Oak Ridge using a straight-walled nozzle with a wedge angle of 15°, in which the temperature is a function of the distance downstream from the throat. The nozzle was exhausted into the purge cascade of the Oak Ridge Gaseous Diffusion Plant, which allowed continuous operation and long spectral scans. The ratio of maximum cross-sectional area of the flow region to that of the throat was 20:1 for this nozzle, but often the data were recorded nearer the throat where the expansion was incomplete, to provide well-resolved spectra at the desired temperature. Records were obtained under a variety of flow conditions; typical values are: mole fraction 0.0015 (i.e., 1.3% depleted UF_6 in Ar), $p_0 = 20$–60 Torr, $T_0 = 300$ K, and $p = 0.3$–2.0 Torr, with $T < 100$ K; but useful spectra were obtained also for conditions outside these ranges. The temperature and number density of the flow were quite reproducible, but usually were not accurately known. Values of these parameters are included in the figure captions where they have been estimated either from the flow characteristics of the expanding gas or from the relative intensities and widths of spectral absorption features.

Spectra were recorded using tunable $Pb_{1-x}Sn_xTe$ semiconductor diode lasers manufactured by Arthur D. Little, Inc., and later by Laser Analytics Inc. (now a division of Spectra-Physics); these provided resolution of better than 10^{-3} cm^{-1} in most regions. The output frequency was adjusted by temperature control of the diode and fine-tuned by varying the current using a ramp generator in addition to the dc bias supply. The laser beam was focused to a spot 2 mm in

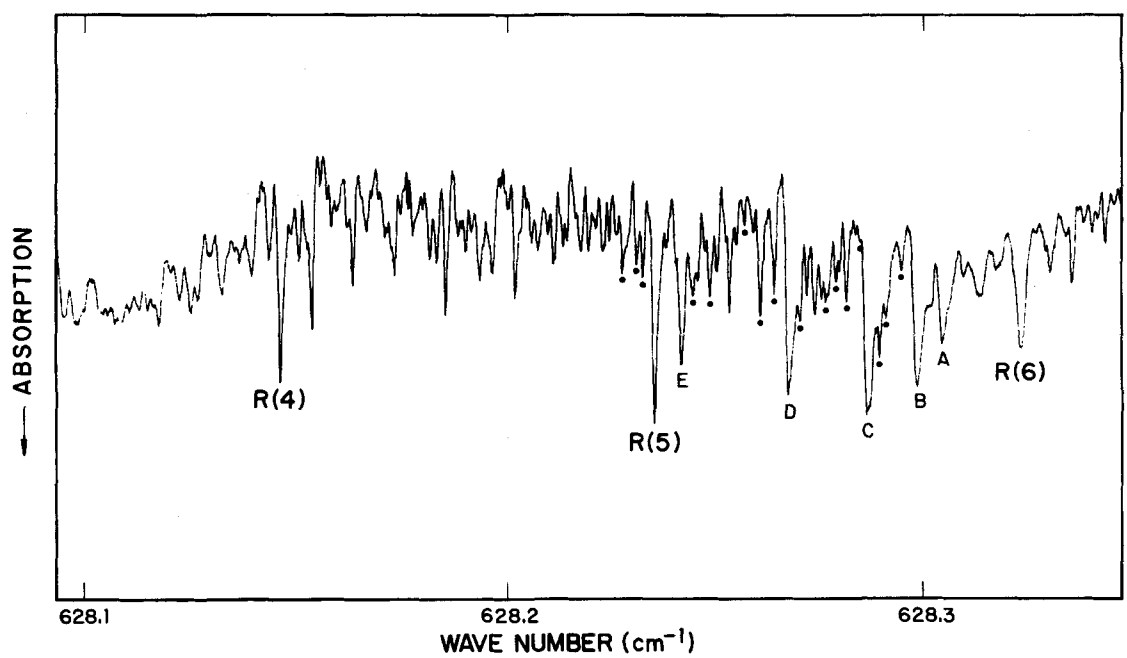

FIG. 6. The R (4) to R (6) region of $^{238}UF_6$, showing the Q branch of $^{235}UF_6$. The relative concentrations of the two species were 95% and 5%, respectively. The subbandheads of the $^{235}UF_6$ Q branch are labeled using the same convention as in Fig. 4 (Refs. 63 and 64); these assignments have been confirmed in other spectra with higher $^{235}UF_6$ concentrations. The 16 absorption features listed in Table III are indicated by the filled circles. Sample was statically cooled to $T \approx 180$ K; path length 400 m.

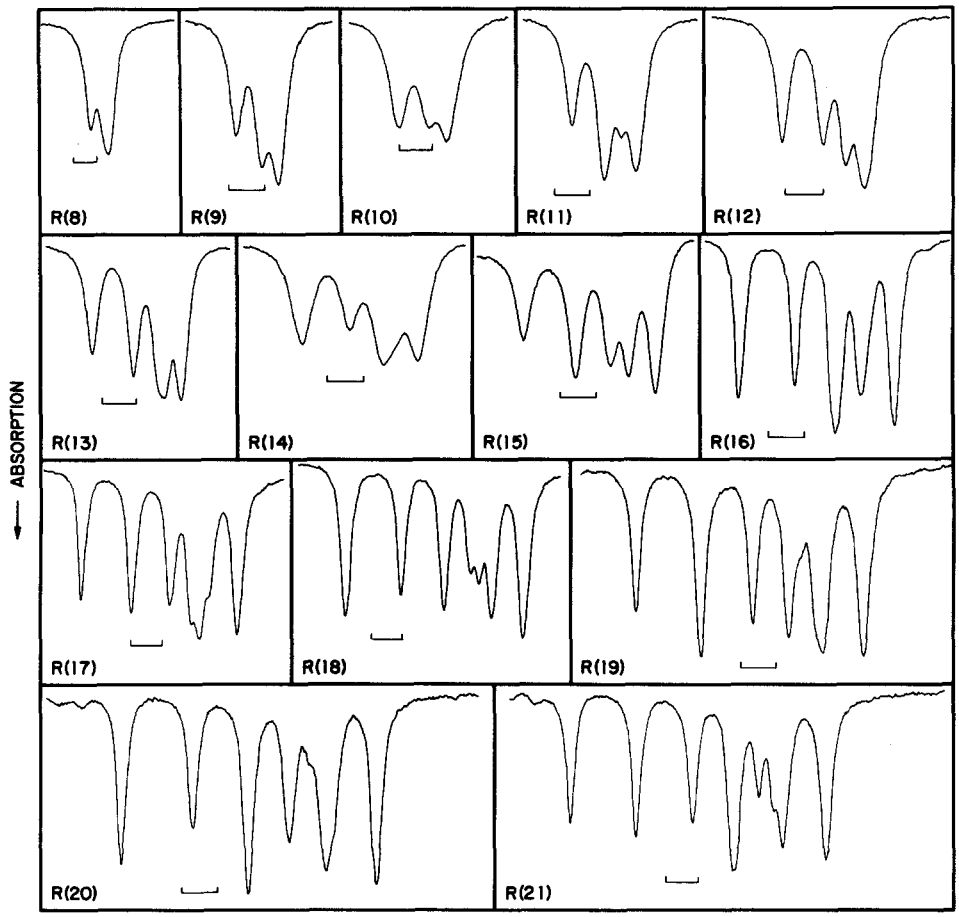

FIG. 7. The $R(8)$ to $R(21)$ manifolds of $^{238}UF_6$. Wave number increases to the right, and the bars beneath each manifold indicate intervals of 0.002 cm^{-1} (60 MHz). At $R(14)$ the resolution of the diode was somewhat degraded. Experimental conditions as for Fig. 1; temperature believed to be near or below 60 K.

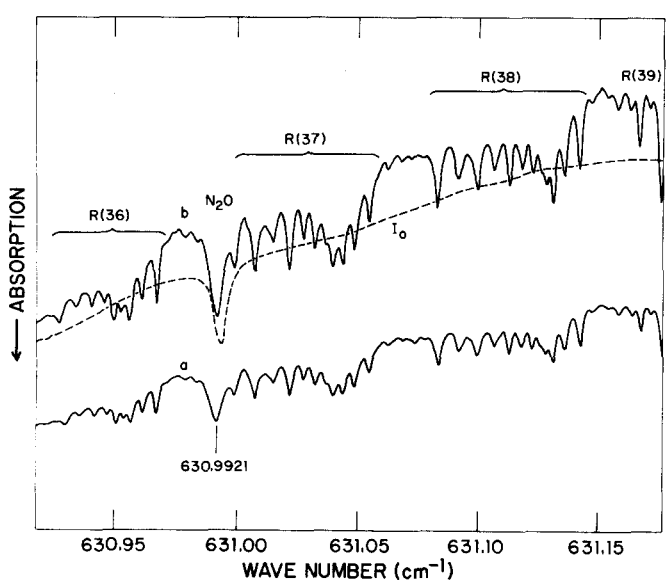

FIG. 8. The $R(36)$ to $R(39)$ region recorded with a calibration line (Ref. 39) of N_2O at 630.9921 cm^{-1}. The I_0 line goes with curve (a) and exhibits a small frequency shift of the N_2O reference line. The strong continuous background absorption in (a) is due to particulate UF_6 and in part to unresolved hot bands. Curve (b) is a rescan with an expanded ordinate. Flow conditions: 2% UF_6 in Ar; temperature and number density unknown; optical path 75 cm.

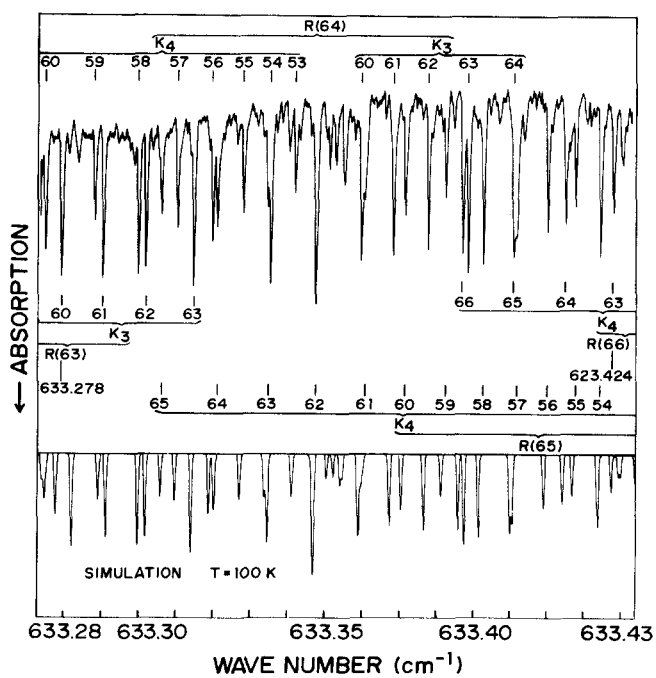

FIG. 9. Portion of the $R(63)$ to $R(66)$ manifolds in $^{238}UF_6$ as observed experimentally and as synthesized using the spectroscopic constants of Table V and a linewidth of 0.0006 cm^{-1} (FWHM). Experimental conditions as for Fig. 1.

diameter, passed through the nozzle viewing area transverse to the flow, mechanically chopped, and then passed through a mode-sorting monochromator to the HgCdTe detector. The signal from the latter was processed with a phase-sensitive PAR lock-in amplifier. The output was displayed on the Y-axis of an X-Y recorder whose X axis was driven by the ramp generator.

UF_6 frequencies were measured relative to ν_2 absorption lines of N_2O. The calculated N_2O frequencies of Olson *et al.*[38] were originally used, but all frequencies given here have been corrected according to the recently reported values obtained with the high-resolution FTIR spectrometer at the University of Oulu.[39] The diode tuning rate was calibrated with germanium etalons having free spectral ranges of typically 0.06 cm^{-1}. Because many of the spectra had to be recorded in laboratories that were not temperature controlled, variable etalon fringe spacing was a problem, with variations as large as $\pm$ 0.005 cm^{-1}/fringe observed under particularly unfavorable conditions. For this reason all measured P- and R-branch UF_6 lines were within 0.04 cm^{-1} (and in most cases within 0.03 cm^{-1}) of an N_2O calibration frequency that had been recorded simultaneously with the UF_6 spectrum.

P- and R-branch lines whose absolute frequencies were measured are listed in Table I, and are identified there by the branch (i.e., the value of ΔJ), the J value of the lower state, and the octahedral fine-structure index according to the convention of Moret-Bailly.[40,41] The manifolds P (11, 20, 29, 38–9, 56–7) and R (7, 17, 27, 37) are covered. Many otherwise useful spectra were recorded in regions further from a calibration line than the criterion of $\pm$ 0.04 cm^{-1} mentioned above, and it was obvious that some of these data could be used to improve the fit of the spectroscopic constants. Accordingly, frequency *differences* between closely spaced lines belonging to different manifolds were measured for P (43–5, 55–9, 70–7) and R (63–7). We selected pairs of lines whose identification was unambiguous and that were separated by no more than about 0.006 cm^{-1}, to minimize etalon errors. Those differences that were included in the analysis are listed in Table II. They were given the same weight as the absolute frequencies in the least-squares regression. The inclusion of the frequency differences greatly improved the overall fit, as will be discussed in the next section.

Only one N_2O calibration line occurs in the UF_6 Q branch. Accordingly, only two directly measured frequencies are listed for this branch in Table I, belonging to Q (38) and Q (53). Most of the Q-branch data were incorporated into the fit by means of frequency differences (Table II) that could be accurately determined from expanded scans with étalon calibrations. We selected pairs of lines satisfying the same criteria as for the P and R branches. Because of the high density of transitions in the Q branch, apparent coincidences of lines are also frequent; where such features appeared in the spectrum as clearly identifiable absorptions whose widths were not significantly greater than those of isolated single transitions, they were entered in the data set with a frequency difference of 0 cm^{-1}.

Most of the difference data for the Q branch consist of separations between very close or nearly coincident Q transitions having different J values, and usually belonging to different subbranches (series of clustered lines) as well. We also sought near coincidences between Q-branch lines and low-J lines in the P and R branches, to ensure consistency between the constant v (which primarily affects the Q branch) and n, p, and h (which concern the P and R branches). This was difficult for several reasons: at temperatures high enough to emphasize the high-J Q-branch transitions, R (0) was too weak to observe; P (3) appears in a region confused by appreciable hot-band absorption; and P (1) was too weak to be identified among the dense Q-branch features even in low-temperature scans such as that of Fig. 5. P (2), however, can be distinguished near identifiable Q-branch lines, and in fact is nearly coincident with the Q_X cluster $Q(54)F_1^2 + E^1 + F_2^2$; these transitions are listed as the first entry in Table II, with a frequency difference of 0 cm^{-1}.

TABLE I. Absolute frequencies used in the fit of the constants.

Identification		ν(cm^{-1}) obs	calc	Δ[a]
P(57)	$F1$(5)	622.4828	622.4823	5
P(57)	$F2$(5)	622.4914	622.4910	4
P(56)	E (9)	622.4945	622.4944	1
P(57)	$F1$(6)	622.4983	622.4986	−3
P(57)	$F1$(7)	622.5050	622.5051	−1
P(57)	$F1$(9)	622.5176	622.5175	1
P(57)	$F2$(10)	622.5260	622.5260	0
P(56)	$F2$(12)	622.5294	622.5295	−1
P(57)	E (7)	622.5325	622.5325	0
P(57)	E (8)	622.5402	622.5402	0
P(56)	$F1$(11)	622.5436	622.5438	−2
P(57)	$F1$(14)	622.5485	622.5487	−2
P(39)	$F1$(9)	624.1893	624.1901	−8
P(38)	E (6)	624.2153	624.2155	−2
P(38)	$F1$(8)	624.2275	624.2270	5
P(29)	$F1$(0)	625.0589	625.0592	−3
P(29)	E (0)	625.0677	625.0675	2
P(29)	$F1$(2)	625.0746	625.0742	4
P(29)	$F2$(2)	625.0799	625.0795	4
P(20)	$F1$(4)	625.8915	625.8917	−2
P(20)	$F1$(3)	625.8970	625.8970	0
P(20)	$F2$(3)	625.9009	625.9009	0
P(20)	E (0)	625.9091	625.9087	4
P(11)	$F1$(0)	626.7123	626.7130	−7
P(11)	$F2$(1)	626.7148	626.7155	−7
P(11)	E (1)	626.7168	626.7177	−9
Q(53)	$F2$(5)	627.5953	627.5946	7
Q(38)	E (0)	627.5977	627.5968	9
R(7)	$A2$(0)	628.4131	628.4129	2
R(17)	$F1$(0)	629.2884	629.2885	−1
R(17)	$F1$(1)	629.2917	629.2919	−2
R(17)	E (2)	629.2978	629.2986	−8
R(27)	$F1$(0)	630.1515	630.1511	4
R(27)	E (0)	630.1577	630.1571	6
R(27)	$F1$(1)	630.1626	630.1622	4
R(27)	$F1$(2)	630.1666	630.1663	3
R(27)	E (3)	630.1756	630.1755	1
R(27)	$F1$(6)	630.1795	630.1794	1
R(37)	$F1$(0)	630.9995	631.0001	−6
R(37)	$A1$(0)	631.0080	631.0085	−5
R(37)	$F1$(2)	631.0159	631.0160	−1
R(37)	$A2$(0)	631.0228	631.0227	1
R(37)	$F1$(3)	631.0286	631.0285	1

[a] $\Delta = (\nu_{obs} - \nu_{calc}) \times 10^4$ cm^{-1}.

TABLE II. Frequency differences used in the fit of the constants.

$\nu_2 - \nu_1$(cm^{-1})				Line 2			Line 1		
J'^a	Ident.		ν_{calc}	J'	Ident.		obs	calc	Δ^b
1	$P(2)$	$F2(0)$	627.5233	54	$Q(54)$	$E(1)$	0.0000	−0.0005	5
19	$Q(19)$	$A2(1)$	627.6804	23	$Q(23)$	$E(1)$	0.0000	−0.0000	0
21	$Q(21)$	$F2(3)$	627.6772	22	$Q(22)$	$F2(2)$	0.0000	−0.0001	1
24	$Q(24)$	F1(5)	627.7067	47	$Q(47)$	F2(1)	0.0000	−0.0000	0
27	$Q(27)$	$F2(5)$	627.6581	31	$Q(31)$	$A2(1)$	0.0000	−0.0000	0
27	$Q(27)$	$F2(5)$	627.6581	36	$Q(36)$	$E(3)$	0.0000	0.0001	−1
27	$Q(27)$	$F1(6)$	627.6495	46	$Q(46)$	$F2(8)$	−0.0006	−0.0007	1
28	$Q(28)$	$F1(6)$	627.7095	30	$Q(30)$	$F2(7)$	0.0016	0.0016	0
28	$Q(28)$	$E(0)$	627.6454	46	$Q(46)$	$F2(8)$	0.0032	0.0033	−1
30	$Q(30)$	$F2(0)$	627.6369	31	$Q(31)$	$E(4)$	−0.0042	−0.0045	3
33	$Q(33)$	$F2(4)$	627.6472	37	$Q(37)$	$E(2)$	0.0000	−0.0000	0
33	$Q(33)$	$F1(0)$	627.7139	54	$Q(54)$	$F1(12)$	0.0000	−0.0002	2
35	$Q(35)$	$E(5)$	627.6129	36	$Q(36)$	$F1(0)$	−0.0054	−0.0052	−2
35	$Q(35)$	$F1(0)$	627.7159	36	$Q(36)$	$F1(8)$	0.0011	0.0011	0
35	$Q(35)$	$F1(4)$	627.6439	39	$Q(39)$	$F2(4)$	0.0000	0.0001	−1
35	$Q(35)$	$F1(4)$	627.6439	53	$Q(53)$	$F1(3)$	0.0000	0.0001	−1
36	$Q(36)$	$F1(8)$	627.7170	37	$Q(37)$	$F1(0)$	0.0011	0.0011	0
36	$Q(36)$	$E(0)$	627.6195	47	$Q(47)$	$F1(4)$	0.0000	−0.0001	1
37	$Q(37)$	$E(5)$	627.6023	46	$Q(46)$	$A2(1)$	−0.0024	−0.0021	−3
37	$Q(37)$	$E(2)$	627.6472	48	$Q(48)$	$E(5)$	0.0000	0.0000	0
38	$Q(38)$	$E(0)$	627.5968	39	$Q(39)$	$F1(9)$	−0.0059	−0.0057	−2
38	$Q(38)$	$F2(6)$	627.6561	42	$Q(42)$	$E(4)$	−0.0039	−0.0039	0
38	$Q(38)$	$F2(9)$	627.7192	59	$Q(59)$	$F2(1)$	0.0005	0.0006	−1
39	$Q(39)$	$F2(6)$	627.6214	46	$Q(46)$	$F1(6)$	0.0000	−0.0002	2
39	$Q(39)$	$F2(6)$	627.6214	57	$Q(57)$	$F1(4)$	0.0000	−0.0000	0
40	$Q(40)$	$E(0)$	627.5852	43	$Q(43)$	$F2(9)$	−0.0036	−0.0039	3
40	$Q(40)$	$F2(3)$	627.6159	49	$Q(49)$	$F1(5)$	0.0000	−0.0000	0
40	$Q(40)$	$F1(9)$	627.7216	60	$Q(60)$	$F1(13)$	−0.0005	−0.0005	0
41	$Q(41)$	$E(6)$	627.5792	43	$Q(43)$	$F2(9)$	0.0024	0.0021	3
42	$Q(42)$	$F1(0)$	627.5731	43	$Q(43)$	$E(6)$	−0.0064	−0.0063	−1
42	$P(43)$	$F1(0)$	623.7420	43	$P(44)$	$E(0)$	−0.0068	−0.0066	−2
42	$Q(42)$	$A2(1)$	627.6106	52	$Q(52)$	$A2(2)$	0.0000	0.0002	−2
43	$Q(43)$	$A2(2)$	627.6066	44	$Q(44)$	$E(3)$	0.0000	−0.0002	2
43	$P(44)$	$F1(10)$	623.6469	44	$P(45)$	$F2(10)$	−0.0027	−0.0025	−2
43	$Q(43)$	$F2(5)$	627.6267	52	$Q(52)$	$F2(9)$	0.0000	−0.0001	1
43	$Q(43)$	$F1(0)$	627.7254	63	$Q(63)$	$F2(1)$	0.0000	−0.0002	2
44	$Q(44)$	$F1(10)$	627.7268	45	$Q(45)$	$F1(0)$	0.0014	0.0014	0
44	$Q(44)$	$E(0)$	627.5603	47	$Q(47)$	$E(6)$	−0.0039	−0.0041	2
45	$Q(45)$	$F2(10)$	627.5537	47	$Q(47)$	$E(6)$	0.0025	0.0025	0
46	$Q(46)$	$E(0)$	627.5470	48	$Q(48)$	$E(0)$	0.0027	0.0026	1
46	$Q(46)$	$E(2)$	627.5863	57	$Q(57)$	$E(3)$	0.0000	−0.0000	0
47	$Q(47)$	$E(5)$	627.5803	50	$Q(50)$	$F1(5)$	0.0000	0.0001	−1
47	$Q(47)$	$F1(4)$	627.6194	59	$Q(59)$	$F2(4)$	0.0000	0.0001	−1
47	$Q(47)$	$F1(0)$	627.7311	67	$Q(67)$	$F2(1)$	0.0000	0.0002	−2
48	$Q(48)$	$F2(0)$	627.5330	50	$Q(50)$	$E(1)$	0.0026	0.0028	−2
48	$Q(48)$	$F1(3)$	627.5742	52	$Q(52)$	$F1(5)$	0.0000	−0.0002	2
48	$Q(48)$	$F1(3)$	627.5742	56	$Q(56)$	$E(5)$	0.0000	−0.0000	0
48	$Q(48)$	$F2(0)$	627.5330	59	$Q(59)$	$E(5)$	−0.0012	−0.0012	0
49	$Q(49)$	$E(7)$	627.5258	51	$Q(51)$	$E(7)$	0.0030	0.0029	1
49	$Q(49)$	$F2(10)$	627.5427	53	$Q(53)$	$F1(10)$	0.0000	−0.0001	1
49	$Q(49)$	$F2(10)$	627.5427	56	$Q(56)$	$F1(5)$	0.0000	−0.0002	2
50	$Q(50)$	$E(0)$	627.5184	53	$Q(53)$	$E(7)$	−0.0045	−0.0045	0
50	$Q(50)$	$F1(5)$	627.5804	60	$Q(60)$	$F1(9)$	0.0000	−0.0000	0
52	$Q(52)$	$F1(12)$	627.7389	53	$Q(53)$	$F1(0)$	0.0016	0.0017	−1
53	$Q(53)$	$A2(2)$	627.5582	54	$Q(54)$	$E(3)$	0.0000	−0.0001	1
54	$P(55)$	$F1(0)$	622.5912	55	$P(56)$	$F1(7)$	0.0012	0.0016	−4
54	$Q(54)$	$F2(0)$	627.4875	56	$Q(56)$	$E(1)$	0.0034	0.0033	1
54	$Q(54)$	$F2(4)$	627.5457	68	$Q(68)$	$F1(10)$	0.0000	−0.0001	1
55	$Q(55)$	$E(8)$	627.4794	57	$Q(57)$	$E(8)$	0.0032	0.0034	−2
55	$Q(55)$	$F1(0)$	627.7440	75	$Q(75)$	$F2(1)$	0.0006	0.0007	−1
56	$P(57)$	$F1(2)$	622.4334	57	$P(58)$	$E(2)$	0.0000	0.0005	−5
56	$P(57)$	$F1(1)$	622.4166	57	$P(58)$	$F1(7)$	−0.0055	−0.0056	1
56	$P(57)$	$F2(2)$	622.4481	57	$P(58)$	$A2(0)$	0.0000	0.0004	−4
56	$Q(56)$	$E(0)$	627.4711	58	$Q(58)$	$F2(1)$	0.0034	0.0035	−1
57	$P(58)$	$F1(11)$	622.3522	58	$P(59)$	$E(8)$	0.0047	0.0046	1
57	$P(58)$	$F1(11)$	622.3522	58	$P(59)$	$F2(12)$	−0.0035	−0.0034	−1
57	$P(58)$	$F1(13)$	622.3200	58	$P(59)$	$F2(7)$	−0.0033	−0,0032	−1
57	$P(58)$	$F2(11)$	622.3654	58	$P(59)$	$E(9)$	0.0000	0.0001	−1

TABLE II. (*Continued*).

Line 1				Line 2			$\nu_2-\nu_1(cm^{-1})$		
J'^a	Ident.		ν_{calc}	J'	Ident.		obs	calc	Δ^b
57	$Q(57)$	E (8)	627.4828	59	$Q(59)$	$F2(12)$	0.0022	0.0019	3
57	$Q(57)$	$F1$(0)	627.7476	77	$Q(77)$	$F1$(1)	0.0007	0.0008	−1
59	$Q(59)$	$F1$(0)	627.7514	79	$Q(79)$	$F2$(1)	0.0007	0.0009	−2
61	$Q(61)$	$F1$(0)	627.7553	81	$Q(81)$	$F1$(1)	0.0008	0.0009	−1
63	$Q(63)$	$F1$(0)	627.7593	83	$Q(83)$	$F2$(1)	0.0008	0.0009	−1
64	$R(63)$	E (9)	633.3016	65	$R(64)$	$F2(11)$	−0.0021	−0.0020	−1
64	$Q(64)$	$F1(15)$	627.7613	65	$Q(65)$	$F1$(0)	0.0020	0.0021	−1
64	$Q(64)$	$F2$(6)	627.4938	81	$Q(81)$	E (4)	0.0000	−0.0001	1
64	$Q(64)$	$F1(15)$	627.7613	84	$Q(84)$	$F1(19)$	0.0007	0.0009	−2
65	$R(64)$	$A2$(1)	633.3590	66	$R(65)$	$F1$(3)	0.0000	−0.0000	0
65	$R(64)$	$F1$(9)	633.3186	66	$R(65)$	$F1$(1)	0.0012	0.0014	−2
65	$R(64)$	$F2$(8)	633.3344	66	$R(65)$	$F1$(2)	−0.0008	−0.0007	−1
65	$R(64)$	$F2$(1)	633.3876	67	$R(66)$	$F2(16)$	−0.0017	−0.0016	−1
65	$Q(65)$	$F1$(0)	627.7634	85	$Q(85)$	E (0)	0.0009	0.0009	0
66	$R(65)$	E (8)	633.4529	67	$R(66)$	$F1(12)$	−0.0009	−0.0009	0
66	$R(65)$	E (10)	633.4863	67	$R(66)$	$F2(10)$	−0.0030	−0.0033	3
66	$R(65)$	$F2(13)$	633.4624	67	$R(66)$	$F1(11)$	0.0008	0.0006	2
67	$R(66)$	$F1(11)$	633.4631	68	$R(67)$	$F1$(0)	0.0028	0.0032	−4
67	$R(66)$	$F1$(9)	633.4917	68	$R(67)$	$F1$(1)	0.0032	0.0033	−1
67	$R(66)$	$F1$(7)	633.5069	68	$R(67)$	$F1$(2)	0.0016	0.0016	0
67	$R(66)$	$F2(10)$	633.4830	68	$R(67)$	$F2$(1)	−0.0022	−0.0020	−2
67	$Q(67)$	$F1$(0)	627.7678	87	$Q(87)$	$F2$(1)	0.0008	0.0009	−1
69	$P(70)$	$F1(14)$	621.1916	70	$P(71)$	$F1$(8)	0.0032	0.0030	2
69	$P(70)$	$F1(16)$	621.1496	71	$P(72)$	E (1)	0.0015	0.0014	1
70	$P(71)$	$F1$(5)	621.1555	71	$P(72)$	E (1)	−0.0045	−0.0045	0
70	$P(71)$	$F1$(4)	621.1426	71	$P(72)$	$F1$(3)	0.0000	−0.0004	4
70	$P(71)$	$F1$(6)	621.1671	71	$P(72)$	$F1$(0)	0.0044	0.0043	1
70	$P(71)$	$F1$(2)	621.0941	71	$P(72)$	$F2(10)$	−0.0026	−0.0029	3
71	$P(72)$	$F1(10)$	621.0817	72	$P(73)$	E (11)	−0.0023	−0.0025	2
71	$Q(71)$	$F1$(0)	627.7768	91	$Q(91)$	$F2$(1)	0.0010	0.0008	2
72	$Q(72)$	$F1(17)$	627.7791	73	$Q(73)$	$F1$(0)	0.0023	0.0024	−1
73	$P(74)$	$F1(16)$	620.7792	75	$P(76)$	E (1)	0.0022	0.0020	2
73	$P(74)$	$F2(18)$	620.7280	75	$P(76)$	$F1$(9)	−0.0016	−0.0020	4
74	$P(75)$	$F1$(5)	620.7696	75	$P(76)$	E (2)	0.0021	0.0022	−1
74	$P(75)$	$F1$(6)	620.7824	75	$P(76)$	E (1)	−0.0008	−0.0011	3
74	$P(75)$	$F2$(4)	620.7397	75	$P(76)$	$F2$(8)	0.0000	−0.0000	0
75	$P(76)$	$F1(11)$	620.6977	76	$P(77)$	E (11)	0.0014	0.0015	−1
75	$P(76)$	$F1(12)$	620.6859	76	$P(77)$	$F1(17)$	0.0025	0.0028	−3
75	$P(76)$	$F2(11)$	620.7082	76	$P(77)$	E (12)	0.0021	0.0021	0
76	$Q(76)$	$F1(18)$	627.7888	77	$Q(77)$	$F1$(0)	0.0026	0.0025	1
79	$Q(79)$	$F1$(0)	627.7965	80	$Q(80)$	$F1(19)$	0.0026	0.0026	0
84	$Q(84)$	$F1(20)$	627.8099	85	$Q(85)$	$F1$(0)	0.0028	0.0028	0

[a] Entries are listed in order of increasing J', the total angular momentum quantum number in the upper state.
[b] $\Delta=[(\nu_2-\nu_1)_{obs}-(\nu_2-\nu_1)_{calc}]\times10^4\ cm^{-1}$.

The Q branch of $^{235}UF_6$, observed between the R (4) and R (6) transitions of $^{238}UF_6$ (Fig. 6), was also recorded and analyzed. From computer syntheses of this Q branch, we could identify in spectra like that of Fig. 6, 24 individual transitions appearing as 16 absorption features. Their wave numbers were measured relative to those of $^{238}UF_6$ R (5) and R (6) using a linear interpolation that was shown to be appropriate from the examination of étalon-calibrated scans from R (4) to R (7); the results are given in Table III.

SPECTROSCOPIC ANALYSIS

The analysis follows the theory of Hecht[42] and Moret-Bailly[40,41] for an infrared-active fundamental band of a rotating, vibrating spherical-top molecule. Spin-statistical weights[43] for the octahedral fine-structure components[44] and the clusterings of these component sublevels[45–49] were crucial to making identifications. Moret-Bailly's formulas[40,41] for the strongly allowed individual rotational lines can be expressed in the form[50]

$$\nu_{P,R}=m+nM+pM^2+qM^3+\cdots+(g-hM+\cdots)\times[(2R-3)(2R-2)\cdots(2R+5)]^{1/2}\times[2M(2M+1)]^{-1}(-1)^R F^{(4,R,R)}_{A_1PP} \quad (1)$$

for the P and R branches, and

$$\nu_Q=m+vJ_0(J_0+1)+\cdots+(-2g+\cdots)\times[(2R-3)(2R-2)\cdots(2R+5)]^{1/2}\times[2J_0(2J_0+2)]^{-1}(-1)^R F^{(4,R,R)}_{A_1PP} \quad (2)$$

for the Q branch. These expressions are equivalent to the "dominant approximation" of Hecht.[42] Here $M=(J_0+1)$

TABLE III. Q-branch transitions in ν_3 of $^{235}UF_6$.

Identification		ν (cm^{-1}) obs	calc	Δ[a]
$Q(33)$	$F2(7)$	628.2265	628.2265	0
$Q(32)$	$E(0)$	628.2311	628.2313	−2
$Q(34)$	$A2(0)$	628.2324	628.2328	−4
$Q(29)$	$E(4)$	628.2451	628.2448	3
$Q(28)$	$E(0)$	628.2488	628.2490	−2
$Q(26)$	$E(0)$	628.2572	628.2569	3
$Q(25)$	$E(3)$	628.2611	628.2606	5
$Q(24)$	$F2(0)$	628.2646	628.2642	4
$Q(22)$	$E(0)$	628.2709	628.2709	0
$Q(23)$	$A2(1)$	628.2771	628.2772	−1
$Q(20)$	$E(0)$	628.2771	628.2770	1
$Q(30)$	$F1(4)$	628.2771	628.2772	−1
$Q(19)$	$E(2)$	628.2798	628.2798	0
$Q(27)$	$F1(2)$	628.2798	628.2798	0
$Q(24)$	$F2(3)$	628.2822	628.2828	−6
$Q(18)$	$A2(0)$	628.2822	628.2828	−6
$Q(17)$	$E(2)$	628.2851	628.2850	1
$Q(24)$	$A2(1)$	628.2901	628.2896	5
$Q(17)$	$A2(0)$	628.2918	628.2913	5
$Q(14)$	$E(0)$	628.2918	628.2917	1
$Q(20)$	$A2(0)$	628.2918	628.2916	2
$Q(12)$	$A2(0)$	628.2956	628.2961	−5
$Q(13)$	$A2(0)$	628.2956	628.2958	−2
$Q(14)$	$E(1)$	628.2956	628.2957	−1

[a] $\Delta = (\nu_{obs} - \nu_{calc}) \times 10^4$ cm^{-1}.

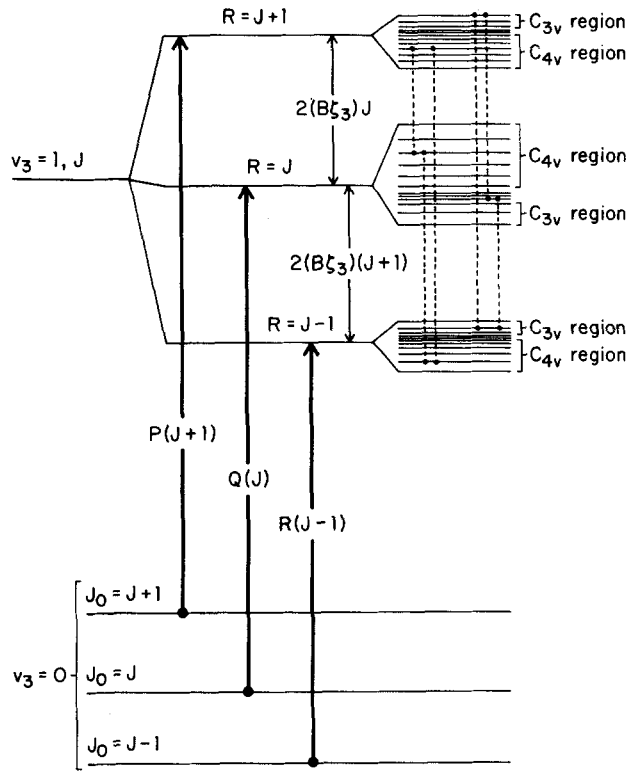

FIG. 10. Strongly allowed ($\Delta R = 0$) P-, Q-, and R-branch transitions in the ν_3 fundamental band of a spherical-top molecule, and the structure of a high-J rotational level in the $v_3 = 1$ excited state. The sketch indicates the Coriolis splitting into three R sublevels for $(B\zeta_3) > 0$ and shows further resolution into the fine-structure manifolds with $g < 0$. The widths of the manifolds are approximately $(700/27)^{1/2} gR^2 \approx 5gR^2$ for $R = J \pm 1$ and twice as large for $R = J$ (Ref. 60). The vertical dashed lines represent interactions that are allowed between the fine-structure components of different R manifolds having the same octahedral symmetry. (For more details see Refs. 49, 60, and 61.) Although $(B\zeta_3)$ does not appear explicitly in the diagonal matrix elements in Eqs. (1) and (2), its value is crucial to the perturbation energies, which depend upon the energy separations between interacting levels. The downward shift by $2(B\zeta_3)$ of the $R = J$ Coriolis sublevel represents the difference between the observed band origin m and the purely vibrational transition ν_3, as given in Eqs. (3) and (4).

for the R branch and $-J_0$ for the P branch, where J_0 refers to the lower state. In Eqs. (1) and (2), R specifies the Coriolis sublevel of the upper state (see Fig. 10). Since $\Delta R = 0$ (or $R = J_0$) in strong dipole transitions of a spherical top, $R = (J+1, J, J-1)$ is associated with the (P,Q,R) branches of the band. Each (J,R) sublevel in the excited state represents a fine-structure manifold, whose individual components are labeled [40,41] by $p = \{C,n'\}$, where C is the octahedral symmetry species ($C = A_1, A_2, E, F_1$, or F_2), and n' is the numerical index distinguishing repeated species within a J manifold. For convenience, the constants used here are compared with those used by other authors in Table IV.

In a "first-order" analysis the terms in Eqs. (1) and (2) involving m, n, p, g, and v are sufficient. At this level of approximation, the positions of lines in a given manifold are proportional[40,41] to the diagonal coefficients $F^{(4,R,R)}_{A_1pp}$ (whose values are given in Refs. 51 and 52), and no matrix diagonalization is necessary. This approximation is insufficient for the present UF_6 data, where the second-order constant h has been determined significantly, and where the fine-structure patterns in the higher-J manifolds are noticeably perturbed from those predicted by the $F^{(4,R,R)}_{A_1pp}$ coefficients alone; this has also been true for the fundamental bands of several other spherical tops including ν_3 of SF_6,[53–55] ν_4 of CF_4,[56] ν_3[57] and ν_4[58] of SiF_4, and ν_{11} and ν_{12} of C_8H_8.[59] In such cases, matrix diagonalization[42] or a higher-order treatment[40,41] is required. These distortions are the result of interactions between the Coriolis sublevels of the $(v_3 = 1, J)$ excited state (see Fig. 10). The form of these perturbations has been discussed.[60,61] In the second- and higher-order approximations, these interactions not only influence the fine structure, but also contribute a scalar shift to the position of each manifold that is comparable to the q term in Eq. (1). To analyze a spectrum that exhibits these effects, one must include terms that depend upon off-diagonal $F^{(4,R,R')}_{A_1pp'}$ coefficients and upon the value of $(B\zeta_3)$, whereas Eqs. (1) and (2) involve only the diagonal (J, R, p) matrix elements. The formalism of Loëte *et al.*[54] for the $(J, R, p; J, R', p')$ off-diagonal elements is particularly convenient for computing the corrections to the line positions. Third-order corrections to the energies have been formulated,[40,41,50,61] but none of these constants could be determined from the present data. In particular, a contribution involving the diagonal sixth-rank $F^{(6,R,R)}_{A_1pp}$ tensor coefficients is a possible third-order effect, but it is insignificant here.

In the present work seven constants were adequate in the fit: $(B\zeta_3)$ and the constants of Eqs. (1) and (2) (excepting q, which was only marginally significant). These constants were fitted to both the 43 absolute frequencies of Table I and the 110 frequency differences of Table II. Rather than making a single simultaneous fit, however, we adopted a some-

TABLE IV. Constants used in the analysis of the ν_3 band.[a]

Present work[b]	Order (Ref. 41)	Moret-Bailly (Ref. 41)	Hecht[c] (Ref. 42)	Robiette *et al.* (Ref. 82)
m (band origin)[d]	0	$\alpha - \alpha^0 + 2\lambda + 6\delta$	$E_{0v} - 2(B\zeta)_{\text{eff}}(v_3 = 1)$	$\nu_3 - 2(B\zeta_3) - \frac{1}{2}\alpha_{220}$
$(B\zeta_3)$	2	$-\lambda$	$(B\zeta)_{\text{eff}}(v_3 = 1) - \frac{1}{4}Z_{3s}$	$B\zeta_3$
n	2	$\beta + \beta^0 - 2(B\zeta_3) + 10\delta$	$B_0 + B'_p - 2(B\zeta_3) - \frac{1}{2}Z_{3s}$	$B_0 + B - 2(B\zeta_3) - \frac{5}{6}\alpha_{220}$
p	4	$\beta - \beta^0 + 4\delta$	$B'_p - B_0 = Y_3 - \frac{1}{3}Z_{3s}$	$B - B_0 - \frac{1}{3}\alpha_{220}$
v	4	$\beta - \beta^0 - 8\delta$	$B'_Q - B_0 = Y_3 + \frac{2}{3}Z_{3s}$	$B - B_0 + \frac{2}{3}\alpha_{220}$
q	6	4γ	$-4D_s$	$-4D$
g	4	ϕ	$-\sqrt{\frac{3}{7}}Z_{3t}$	$-\sqrt{\frac{12}{7}}\alpha_{224}$
h	6	$4\mu - 16\epsilon$	$\sqrt{\frac{12}{7}}(-F_{3t} + 4D_t)$	$\sqrt{\frac{12}{7}}(F_{134} + D_{044})$
$(2p + v)/3$		$\beta - \beta^0$	Y_3	$-\alpha \equiv B - B_0$
$v - p$		-12δ	Z_{3s}	α_{220}
$B_0 + p$		$\beta + 4\delta$	B'_p	$B - \frac{1}{3}\alpha_{220}$
$B_0 + v$		$\beta - 8\delta$	B'_Q	$B + \frac{2}{3}\alpha_{220}$
$B_3 \equiv B'$		β	$B_0 + Y_3$	B

[a] The first eight of these parameters were actually fitted to the data. The remaining five are listed here to clarify the relations between the symbols used by various authors.

[b] This set of symbols is consistent with the spectroscopic notation of Bobin and Fox (Ref. 50) and was chosen because the diagonal matrix elements [given in Eqs. (1) and (2)] are simplified.

[c] For convenience we have abbreviated Hecht's symbols $B_{\text{eff}}(v = 1, R = J \pm 1)$ to B'_p, $B_{\text{eff}}(v = 1, R = J)$ to B'_Q, and $B_{\text{eff}}(v = 0)$ to B_0. The term $+\frac{1}{4}Z_{3s}$ in Hecht's effective $(B\zeta_3)$ represents a small contribution from the scalar O_{PP33} operator (see Table V in Ref. 42). It is *not* included in our effective $(B\zeta_3)$.

[d] This is the point in the band represented by $M = 0$ in Eq. (1) or $J_0 = 0$ in Eq. (2), although no absorbing transition occurs at precisely this wave number. The quantity $(\alpha - \alpha^0)$, E_{0v}, or ν_3 indicates the "purely vibrational" wave number and includes the anharmonic shifts due to terms like $X_{33}(\mathbf{p}_{3x}^2 + \mathbf{q}_{3x}^2)^2$ and $G_{33}\mathbf{l}_3^2$, as well as the harmonic contribution (cf. Ref. 42).

what different approach. We note that the inclusion of difference frequencies cannot affect the zeroth-order constant m (as m cancels out of a frequency difference), and their influence on the constants n and p was found to be negligible (because our P- and R-branch data contain no region in which more than three J manifolds overlap). The differences do, however, improve the determination of the remaining constants. Accordingly, the seven significant parameters reported in the top section of Table V were obtained from a sequence of fits as follows: (1) a seven-parameter fit to all 153 frequencies and frequency differences; (2) a four-parameter fit of $B\zeta_3$, g, h, and v to the 110 differences, fixing m, n, and p at the values found in (1); (3) a three-parameter fit of m, n, and p to all 153 frequencies, fixing $B\zeta_3$, g, h, and v at the values found in (2); and (4) a repetition of step (2) with m, n, and p held at the values found in (3). Each of the four fits involved an iterative nonlinear least-squares reduction of the free parameters, and during each iteration the computer performed a diagonalization of the vibration-rotation Hamiltonian in the (J,R,C) symmetry subspace for the upper state of each observed transition.

The convergence to final values of the seven parameters was rapid, as changes in the constants were all much smaller than one standard deviation after step (2). This approach permitted us to utilize the more accurate difference data in fits of $B\zeta_3$, g, h,and v alone. As a result, the standard deviations in these four parameters were all reduced by about 30% compared with a simultaneous fit of all parameters to all 153 data points. (Table V presents these lower standard deviations.) Also, the standard deviation of the overall fit fell from 0.000 27 cm^{-1} for the seven-parameter fit (as given in Table V) to 0.000 18 cm^{-1} for the four-parameter fit to difference data alone.

We will now discuss some of the features that appear in the observed spectra, Figs. 1–9, and the details of the analysis. For our temperatures and pressures, rotational manifolds in the P and R branches begin to reveal octahedral fine structure at about (upper state) $J = 9$, as shown in Fig. 7. The manifolds widen approximately quadratically[62] with J and start to overlap each other at P (45–46) and R (45–46). In the high-J regions of Figs. 1, 2, and 9, a compact notation for clustered eigenvalues[47–49] is appropriate for the identification of octahedral fine-structure components. There each cluster is labeled by the index K_3 or K_4 that represents the quantized component of the angular momentum $\mathbf{R}$ in the directions of the molecular axes of trigonal C_{3v} or tetragonal C_{4v} symmetry, respectively, in units of $\hbar$. This index assumes the values $K = R, R-1, R-2, \cdots$, for successive clusters, with $K = R$ for the cluster at either end of the manifold.

The extensively overlapped high-J regions in the P and R branches were synthesized at several points in the analysis to ensure that the assignments were correct and that the spectroscopic constants were converging to proper values. Examples of such spectral simulations, using the final constants of Table V, are shown in Fig. 2 for P (54–58) and in Fig. 9 for R (63–66). Note that the latter region is some 2.3 cm^{-1} above the highest-frequency absolutely calibrated R-branch lines at R (37), but the additional frequency-difference data that we have used (Table II) yields a set of molecular constants that reproduce this region, and the whole ν_3 spectrum, with excellent fidelity. Supplementing absolute frequencies with frequency differences is a technique that should be gen-

TABLE V. Constants for ν_3 of UF_6.[a]

Constant	$^{8}UF_6$ Present work	$^{8}UF_6$ Takami *et al.*[b]	$^{235}UF_6$[c]
Spectroscopic constants, fitted to measured frequencies			
m	627.701 78(7)	627.701 92(15)	628.305 37(15)
n	0.089 206 1(16)	0.089 259(12)	
$(B\zeta_3)$	0.011 05(4)[d]	0.011 034(6)[e]	c
$p\times10^5$	− 3.978(5)	− 3.17(10)	
$v\times10^5$	− 3.7208(20)	...	− 3.74(3)
$q\times10^8$	0[f]	9(2)	
$g\times10^6$	− 9.312(3)	− 9.17(9)	− 9.26(6)
$h\times10^9$	− 3.47(4)	...	
Derived molecular constants			
$\nu_3 = m + 2(B\zeta_3) + \frac{1}{2}(v-p)$	627.723 87(11)	627.723 99(15)	628.327 67(17)[g]
$Z_{3s} = v - p$	2.58(5)$\times10^{-6}$		
$B_3 - B_0 = Y_3 = \frac{1}{3}(2p+v)$	− 3.893(3)$\times10^{-5}$		
$B_3 + B_0 = n + 2(B\zeta_3) + \frac{5}{6}(v-p)$	0.111 30(9)		
$B_0 = \frac{1}{2}n + (B\zeta_3) + \frac{1}{4}(v-3p)$	0.055 67(4)		
$B_3 = \frac{1}{2}n + (B\zeta_3) + \frac{1}{12}(7v-p)$	0.055 63(4)		
Statistics			
N = no. of frequencies	153($J\leqslant91$)	154($J\leqslant27$)	24($J\leqslant34$)
σ	0.000 27	0.000 6	0.000 34

[a] All constants are in cm^{-1}. Standard deviations of the parameters are given in parentheses, in units of the last figure quoted.
[b] Reference 35. They apparently fitted $m, n, p, q = -2(D_3 + D_0)$, s, and g, where $s = D_0 - D_3$ is the coefficient of the M^4 scalar term in Eq. (1). We do not find s to be significant in the fit even at high J.
[c] Only the Q branch was analyzed; $(B\zeta_3)$ was constrained at the $^{238}UF_6$ value.
[d] Fitted value, determined mainly by the off-diagonal contributions at high J.
[e] Calculated from n and p by assuming $B_0 = 0.055\ 68\ cm^{-1}$ as obtained from the electron-diffraction bond length of Kimura *et al.* (Ref. 69). The uncertainty in the $(B\zeta_3)$ of Takami *et al.* is actually much greater than the figure quoted, for the latter does not reflect the uncertainty in the assumed value of B_0: The error limit for r (Ref. 69) translates to $\pm 0.0004\ cm^{-1}$ in B_0, which is then also the uncertainty in the calculated value of $(B\zeta_3)$.
[f] This constant is of marginal significance; allowing it to float results in $q = -3.5(17)\times10^{-9}\ cm^{-1}$, with very minor changes in the other constants.
[g] This is the sum of m for $^{235}UF_6$, $2(B\zeta_3)$ for $^{238}UF_6$, and the correction term $2\Delta\ (B\zeta_3) \approx 0.000\ 20\ cm^{-1}$; see the text for discussion.

erally useful in laser spectroscopy, where adequate closely spaced calibration lines are not always available.

The Q branch contains several strong, sharp subband-heads, so that its structure belongs to category (ii) of Brock *et al.*[63] for fundamental bands. These subbandheads correspond to accumulations of C_{4v} clusters of lines and are labeled A, B, and C in Fig. 4, following the conventions of Refs. 63 and 64. The value of $\beta \equiv v/g$ is + 4.00, and a simulation of such a Q branch was given in Fig. 5A of Ref. 63. On the high-frequency side of the band origin the strong regular pattern with alternating line intensities is the A series, accompanied by smaller contributions from higher-J lines in the B series. Early assignment of this structure helped to extend the computer simulations and the fit to high J on the low-frequency side. The present constants predict that the $R(0)$ line lies 0.0005 cm^{-1} below the Q_A cluster $Q(77)$ $F_1^{(0)} + F_2^{(0)}$.

SPECTROSCOPIC AND MOLECULAR CONSTANTS

Table V gives for $^{238}UF_6$ the values determined for the scalar constants m, n, p, v, and the tensor constants g, h of Eqs. (1) and (2). The inclusion of carefully calibrated high-J data has enabled us to report also $(B\zeta_3)$, which is determined in our fit primarily from the effect of the off-diagonal contributions. The frequency differences of Table II allowed this fit of $(B\zeta_3)$, which to our knowledge has not been accomplished in other analyses of vibrational fundamentals of heavy spherical-top molecules.

With $(B\zeta_3)$ known, and distinguishable as a separate contribution to the spectroscopic constant n (see line 3 in Table IV), the ground- and excited-state rotational constants B_0 and B_3 can be obtained directly from the spectroscopic constants n, p, and v, and these are given in Table V. The individual determination of these constants is possible in light spherical tops such as CH_4 from the analysis of forbidden ($\Delta R \neq 0$) transitions. For heavy spherical tops, where such lines are too weak to be seen,[49] B_0 can be determined with the aid of overtone bands, in which strong Coriolis interaction allows one to obtain $B\zeta$; this has been done for $3\nu_3$ of SF_6[65] and SiF_4.[66] B_0 of CF_4 has also been reported[67] from an analysis of the $\nu_2 + \nu_4$ combination band, in which branches forbidden in the fundamental become allowed. UF_6 is believed to be the first case in which $B\zeta$, B_0, and B' have been determined with reasonable accuracy from only the allowed transitions in a vibrational fundamental.

The U–F bond length in the ground vibrational state, obtained from B_0, is

$$r_0 = 1.9962 \pm 0.0007\ \text{Å}.$$

This agrees with, but is more precise than, the most recent electron diffraction measurements of 1.999 ± 0.003 Å (Seip,[68] quoting the standard deviation) and 1.996 ± 0.008 Å (Kimura *et al.*,[69] quoting the estimated lim-

it of error). The latter values, of course, represent the bond length averaged over the many vibrational states that are populated at the temperature of the experiment.

VIBRATIONAL PARAMETERS AND INTRAMOLECULAR FORCE FIELD

The currently preferred values for the observed frequencies ν_i, and the anharmonicity constants X_{ij} for $^{238}UF_6$ are summarized in Table VI; the sources of these data are listed in the footnotes to that table. To calculate the intramolecular force field we need the harmonic frequencies ω_i that are related to the observed frequencies by [70]

$$\nu_i = \sum_i \omega_i v_i + \sum_i X_{ii} v_i(v_i + d_i) + 1/2 \sum_i \sum_{j \neq i} X_{ij} v_i(v_j + d_j), \quad (3)$$

where v_i is the vibrational quantum number and d_i the degeneracy of the fundamental i. This expression neglects second-order shifts of the vibrational levels and splittings into octahedral sublevels[42]; while these effects should in principle be considered,[58] there is not yet enough information on most of the vibrational levels of UF_6 to justify their inclusion. The neglected terms are small and their effects have been considered whenever possible in assigning estimated errors to the ω_i given in Table VI.

The constraints used in fixing the three symmetry force constants in the 2×2 F_{1u} block are the Coriolis constant ζ_3 and the $^{235}UF_6$–$^{238}UF_6$ isotope shift in ν_3. The first of these is approximated by

$$\zeta_3 \approx (B\zeta_3)/B_3 = 0.1986(7).$$

The actual way in which ζ enters into the spectroscopic constant n is more complex than this, and has been considered in detail for tetrahedral molecules by Hecht.[42] We have

$$(B\zeta_3)_{\text{eff}} = B_e\zeta_3 + \text{terms in } M_{3ii} \quad (i = 1 \text{ to } 6),$$

where the M_{3ii} are third-order interaction constants that express the change in the effective Coriolis interaction in various vibrational states, and which are complicated functions of the cubic and quartic potential constants. The M's are small, but there is evidence in SF_6 that their total contribution is not negligible,[71] and in any case B_e is not yet known for UF_6. Lacking any direct information on the extent of the correction, we have taken $\zeta_3 = 0.199(2)$ for the purposes of the force field calculation.

The $^{235}UF_6$–$^{238}UF_6$ isotope shift in ν_3 is known to be about 0.6 cm^{-1}.[11,14,15,21,30,31,72,73] The diode data of Takami *et al.*[35] and the present work provide a much more accurate value; we find the isotope shift in m to be $\Delta m = 0.603\,59(17)$ cm^{-1}, in excellent agreement with 0.6038 cm^{-1} reported by Takami *et al.*[35] Since (cf. Table IV)

$$m = \nu_3 - 2(B\zeta_3) - \tfrac{1}{2}(v - p), \quad (4)$$

we can write

TABLE VI. Vibrational parameters of $^{238}UF_6$.[a]

	$i=1$	$i=2$	$i=3$	$i=4$	$i=5$	$i=6$
Γ_i	A_{1g}	E_g	F_{1u}	F_{1u}	F_{2g}	F_{2u}
ν_i	668.2(3)[b]	534.5(10)[c]	627.7239[d]	187.5(10)[e]	201(2)[f]	143(3)[f]
ω_i[g]	673(2)	541(3)	636(2)	189(3)	202(3)	144(3)
X_{1i}	−0.2(3)[f,h]	−1.5(6)[f,h,i]	−1.6(3)[f,i,j]	−0.2(2)[i]	$-0.2_5(2_0)$[i]	−0.1(1)[i]
X_{2i}	...	−0.3(7)[f]	−2.7(7)[f]	[−0.3][k]	[−0.2][k]	[−0.1][k]
X_{3i}	...	...	−0.9(4)[f,h,l]	−0.3(3)[m]	−0.3(3)[m]	−0.2(2)[m]
ζ_i	(0)	(0)	0.199(2)[d]	0.29(3)[f]	(−1/2)	(−1/2)
$\Delta\nu_i$(235–238)	...	...	0.60379(17)[d]	[0.206][n]	...	...
$\Delta\omega_i$(235–238)	(0)	(0)	0.6157(33)[d]	[0.208][n]	(0)	(0)

[a] Units are cm^{-1} except for ζ_i, which is dimensionless; estimated error limits, in units of the last figure quoted, are given in parentheses.

[b] Measured at the high-frequency edge of the Q branch in the spectrum of Cahen-de Villardi *et al.* (Ref. 23) and corrected for the effect of the apparatus function (0.5 cm^{-1}). (This procedure gives a very close approximation to the true ν_1 band origin of SF_6.)

[c] Q-branch peak given as 532.8 (Ref. 23) and 534.1(5) (Ref. 14) cm^{-1}; the true band origin will be about 1 cm^{-1} to higher frequency. A remeasurement of the Raman spectra reported in Ref. 14 gave for the high-frequency edge of the Q branch, corrected for the apparatus function (5.2 cm^{-1}), 534.9 cm^{-1}.

[d] This paper.

[e] Remeasurement of the infrared spectra of Ref. 14 at the high-frequency edge of the Q branch, corrected for the apparatus function (0.7 cm^{-1}).

[f] McDowell, Asprey, and Paine (Ref. 14). Because of the difficulty in estimating the band origins, the uncertainties in ν_5 and ν_6 were increased slightly from those reported in that paper; ν_5 was remeasured on the high-frequency side of the Q branch.

[g] Calculated from Eq. (3). For this calculation, the bending anharmonicities were estimated by scaling from SF_6 values where possible (see footnote k): $X_{44} = X_{45} = X_{55} = -0.1(2)$; $X_{46} = X_{66} = 0.0(2)$; $X_{56} = -0.2(2)$ cm^{-1}.

[h] Maier, Holland, and Beattie (Ref. 21) give $X_{11} = -0.12(30)$, $X_{12} = -1.24(70)$, and $X_{33} = -1.06(6)$ cm^{-1}, based on measurements of combinations and overtones in solutions of UF_6 in liquid Xe.

[i] Cahen-de Villardi *et al.* (Ref. 23) give $X_{12} = -1.8(3)$, $X_{13} = -1.6(3)$, $X_{14} = -0.2(1)$, $X_{15} = -0.25(10)$, and $X_{16} = -0.10(5)$ cm^{-1}, as estimated from the unresolved Raman contour of ν_1. Their error estimates on X_{14}, X_{15}, and X_{16} have been increased somewhat.

[j] An unpublished high-resolution (Doppler-limited) analysis of $\nu_1 + \nu_3$ yields a band origin of 1294.328 cm^{-1}, from which $X_{13} = -1.6(3)$ cm^{-1}; see Ref. 83.

[k] Very approximate values, obtained by scaling the corresponding constants of SF_6 according to $X_{ij} = X_{ij}^*(\nu_i\nu_j/\nu_i^*\nu_j^*)$, where the asterisks indicate SF_6 values (Ref. 71). In most cases where it can be checked, this formula gives a not unreasonable approximation to the UF_6 anharmonicity constants. Uncertainties are probably ± 0.3 cm^{-1}.

[l] An unpublished high-resolution (Doppler-limited) analysis of $3\nu_3$ yields $X_{33} \approx -0.8$ cm^{-1}; cf. Refs. 79 and 84, which quote a preliminary value of -0.95 cm^{-1}.

[m] Krohn and Kim (Ref. 34) estimate $X_{34} \approx -0.26$, $X_{35} \approx -0.26$, $X_{36} \approx -0.17$ cm^{-1}, from tunable diode laser spectra of the hot bands accompanying ν_3.

[n] Calculated from the force field derived in this paper. The only direct measurement of $\Delta\nu_4$, in Ref. 14, is not very accurate: 0.16 ± 0.12 cm^{-1}. The combination bands $\nu_1 + \nu_4$ and $\nu_2 + \nu_4$ exhibit shifts of 0.2 ± 0.1 cm^{-1} (Ref. 15).

TABLE VII. Force constants of UF_6 (mdyn/Å).[a]

A. Determination of the off-diagonal force constant F_{34}	
$\Delta\omega_3 = 0.6157(33)\ cm^{-1}$	− 0.058(6)
$\zeta_3 = 0.199(2)$	− 0.055(3)
Weighted average	− 0.056(3)
B. Symmetry force constants	
$F_{11} = f_r + 4f_{rr} + f'_{rr}$	5.07(3)
$F_{22} = f_r - 2f_{rr} + f'_{rr}$	3.28(4)
$F_{33} = f_r - f'_{rr}$	3.855(25)
$F_{44} = f_\alpha + 2f_{\alpha\alpha} - 2f''_{\alpha\alpha} - f'''_{\alpha\alpha}$	0.160(5)
$F_{34} = 2(f_{r\alpha} - f''_{r\alpha})$	− 0.056(3)
$F_{55} = f_\alpha - 2f'_{\alpha\alpha} + f'''_{\alpha\alpha}$	0.114(3)
$F_{66} = f_\alpha - 2f_{\alpha\alpha} + 2f''_{\alpha\alpha} - f'''_{\alpha\alpha}$	0.116(5)
C. Valence force constants	
f_r	3.865(19)
f_{rr} (adjacent bonds)	0.299(8)
f'_{rr} (opposite bonds)	0.009(19)
$f_\alpha - f'_{\alpha\alpha}$	0.126(2)
$f_\alpha - f'''_{\alpha\alpha}$	0.138(4)
$f_{\alpha\alpha} - f''_{\alpha\alpha}$	0.011(2)
$f_{r\alpha} - f''_{r\alpha}$	− 0.028(2)

[a] See Ref. 74 for notation and units.

$$\Delta\nu_3 \approx \Delta m + 2\Delta\,(B\zeta_3),$$

$$2\Delta\,(B\zeta_3) \approx 2B_3\Delta\zeta_3 \approx 0.000\,20\ cm^{-1}.$$

This yields a purely vibrational shift $\Delta\nu_3 = 0.603\,79(17)\ cm^{-1}$; this is then converted to $\Delta\omega_3 = 0.6157(33)\ cm^{-1}$ as described in Refs. 14 and 58.

The use of these data to calculate the general quadratic force field of UF_6 is summarized in Table VII.[74] The values of F_{34} determined by ζ_3 and $\Delta\omega_3$ are in good agreement, and using them we have derived in Table VII force constants that are a considerable improvement in precision over those reported in 1974,[14] though the previous constants were correct to within their estimated uncertainties. The resulting eigenvectors and the potential energy matrix are given in Table VIII.

The Cartesian displacement coordinates for the fundamentals ν_3 and ν_4 (the only ones whose form depends upon the intramolecular force field) are shown in Fig. 11 and compared with those of SF_6.[71] In both molecules ν_3 is almost entirely a stretching mode and ν_4 is almost entirely a bend, with even less stretching character in UF_6 than in SF_6. This is consistent with the potential energy distribution of Table VIII.

The vibrational amplitudes calculated from the frequencies of Table VI and the force field of Table VII differ only trivially from those reported in Ref. 14. For a temperature of 300 K, these quantities are now: u(U–F) = 0.0421(1) Å, u(F ··· F, short) = 0.1216(11) Å, and u(F ··· F, long) = 0.0591(2) Å. The shrinkage effects are δ(F ··· F, short) = 0.001 55(5) Å and δ(F ··· F, long) = 0.008 14(19) Å.

TABLE VIII. Eigenvectors and potential energy matrix elements.

	$\omega_3 = 636\ cm^{-1}$	$\omega_4 = 189\ cm^{-1}$
$L_3(amu^{-1/2})$	0.2468	0.0103
$L_4(amu^{-1/2})$	− 0.0832	0.3633
V_{33}	0.986	0.019
V_{44}	0.005	1.000
V_{34}	0.010	− 0.020

DISCUSSION

The combination of flow cooling and tunable laser spectroscopy yields resolved ground-state ($\nu_3 \leftarrow 0$) spectra of UF_6 that would be nearly impossible to obtain by conventional

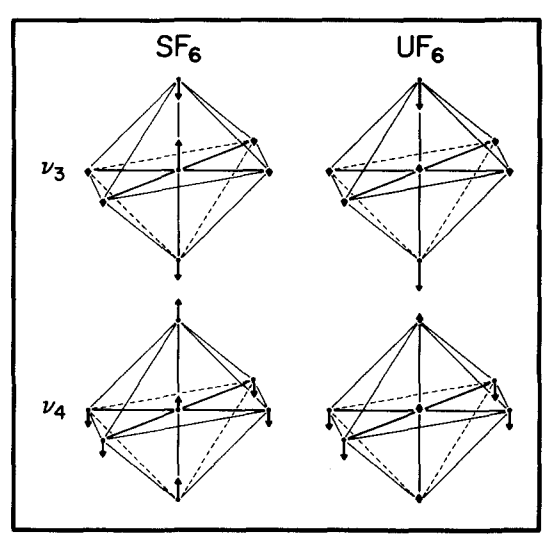

FIG. 11. One component of the triply degenerate F_{1u} normal vibrations of SF_6 and UF_6 as determined from the general quadratic force fields. The normalized, orthogonal vector displacements for the central atom, the two axial F atoms, and the four equatorial F atoms are, respectively, (0.140, –0.098, –0.010) for ν_3 and (0.070, 0.099, –0.079) for ν_4 of SF_6; and (0.025, –0.149, –0.004) for ν_3 and (0.027, 0.034, –0.101) for ν_4 of UF_6, all in units of $amu^{-1/2}$. For ν_3 the displacements of the equatorial F atoms for both molecules have been exaggerated for clarity.

spectroscopic techniques. When the normally present hot-band interferences are thus suppressed, the band proves to have the regular structure that is expected on theoretical grounds for spherical-top molecules and that has been previously observed in such disparate species as CH_4, SiH_4, GeH_4, CF_4, SiF_4, OsO_4, SF_6, MoF_6, WF_6, and C_8H_8.

We wish to emphasize the advantages of including frequency differences together with the frequencies themselves in a polynomial fit of the spectroscopic constants. In the present work we were able to fit $B\zeta_3$ accurately only when these differences were included, so that an expedient that was originally adopted to compensate for lack of sufficient calibration points was found to confer unexpected benefits in the statistical fit. The reasons for this are twofold. First, measurement of closely spaced or coincident lines can be made with great accuracy: the estimated uncertainty in the frequency differences of Table II is of the order of 0.0002 cm^{-1}, which is significantly better than the absolute frequencies of Table I, as an examination of the residuals will show. Second, for that portion of the data set that consists of differences, the zeroth-order constant m is eliminated from the fit, which is then more sensitive to the smaller constants.

It is of interest that among the increasing number of heavy spherical-top molecules that have been studied by high-resolution techniques over the last few years, some regularities are beginning to emerge. We note the close similarity, in appearance and in the values of v and g, between the ν_3 Q branch of UF_6 ($\beta \equiv v/g = 4.00$) and those of $^{96}MoF_6$ ($\beta = 3.9$)[75] and $^{186}WF_6$ ($\beta = 4.25$),[76] despite the fact that the bonding in this series of molecules, as evidenced by their force constants, is quite different.[77] SF_6, a much lighter hexafluoride, has $\beta = 2.84$,[55] not far removed from the above values, and has a generally similar ν_3 Q branch. A similar regularity exists between the tetrafluorides CF_4 and SiF_4, for which the stretching-mode β's are -8.63[78] and -9.07,[57] respectively. The fine structures of bending fundamentals do not seem to follow these regularities.

The analysis of ν_3 is, of course, simply the first step in elucidating the $n\nu_3$ ladder, and further work on this aspect of UF_6 spectroscopy will be reported elsewhere. It is already known[79] that the multiphoton absorption ladders differ greatly among different spherical-top molecules. The heavy central atom in UF_6 results in the three degenerate components of ν_3 being uncoupled, so the major splittings of a given $n\nu_3$ level can be described with separate quantum numbers n_x, n_y, and n_z for each of the three orthogonal motions. In this case the motions can be considered to be local modes rather than normal modes of the molecule as a whole.[80] For the smaller SiF_4 molecule, the orthogonal vibrational motions are strongly coupled by anharmonicity, and the vibrational angular momentum l is a good quantum number with which to label the $n\nu_3$ energy levels.[81] SF_6 is intermediate between these two cases.[65,67,79] The significance of such differences in determining the photochemical behavior of various molecules is just beginning to be explored.

ACKNOWLEDGMENTS

The authors thank J. H. Birely, C. D. Cantrell, T. P. Cotter, R. J. Jensen, O. P. Judd, J. G. Marinuzzi, C. P. Robinson, and S. D. Rockwood of Los Alamos and G. J. Kidd of Oak Ridge for their support and encouragement during the course of this work. The development of the flow-cooling capability would have been impossible without the engineering efforts of D. B. Fradkin and J. A. Sullivan. H. J. Shepard and H. G. Shirley prepared the illustrations. The first 16 μm semiconductor diode lasers used in this work were constructed by K. W. Nill.

[1] R. J. Jensen, J. G. Marinuzzi, C. P. Robinson, and S. D. Rockwood, Laser Focus **12**(5), 51 (May 1976).
[2] R. J. Jensen and C. P. Robinson, AIChE Symp. Ser. **73**, No. 169, 76 (1977).
[3] C. P. Robinson and R. J. Jensen, in *Uranium Enrichment*, edited by S. Villani (Springer, Berlin, 1979), pp. 269–290.
[4] J. W. Eerkens, Appl. Phys. **10**, 15 (1976).
[5] J. J. Tiee and C. Wittig, Opt. Commun. **27**, 377 (1978).
[6] P. Rabinowitz, A. Stein, and A. Kaldor, Opt. Commun. **27**, 381 (1978).
[7] J. A. Horsley, P. Rabinowitz, A. Stein, D. M. Cox, R. O. Brickman, and A. Kaldor, IEEE J. Quantum Electron. **QE-16**, 412 (1980).
[8] J. Subbiah, S. K. Sarkar, K. V. S. Rama Rao, and J. P. Mittal, Indian J. Phys. **54 B**, 121 (1980).
[9] F. S. Becker and K. L. Kompa, Nucl. Tech. **58**, 329 (1982).
[10] G. Meyer-Kretschmer and H. Jetter, Naturwissenschaften **70**, 7 (1983).
[11] M. Alexandre, M. Clerc, R. Gagnon, M. Gilbert, P. Isnard, P. Nectoux, P. Rigny, and J.-M. Weulersse, J. Chim. Phys. **80**, 331 (1983).
[12] P. Rabinowitz, A. Kaldor, A. Gnauck, R. L. Woodin, and J. S. Gethner, Opt. Lett. **7**, 212 (1982).
[13] G. Koren, Y. Gertner, and U. Shreter, Appl. Phys. Lett. **41**, 397 (1982).
[14] R. S. McDowell, L. B. Asprey, and R. T. Paine, J. Chem. Phys. **61**, 3571 (1974).
[15] D. M. Cox and J. Elliott, Spectrosc. Lett. **12**, 275 (1979).
[16] D. M. Cox and A. Gnauck, J. Mol. Spectrosc. **81**, 207 (1980).
[17] R. T. Paine, R. S. McDowell, L. B. Asprey, and L. H. Jones, J. Chem. Phys. **64**, 3081 (1976).
[18] E. Catalano, R. E. Barletta, and R. K. Pearson, J. Chem. Phys. **70**, 3291 (1979).
[19] L. H. Jones and S. A. Ekberg, J. Chem. Phys. **71**, 4764 (1979).
[20] R. F. Holland and W. B. Maier II, Spectrosc. Lett. **16**, 409 (1983).
[21] W. B. Maier II, R. F. Holland, and W. H. Beattie, J. Chem. Phys. **79**, 4794 (1983).
[22] J. Cahen, M. Clerc, P. Isnard, P. Rigny, and J. M. Weulersse, in *Nonlinear Behavior of Molecules, Atoms, and Ions in Electric, Magnetic, or Electromagnetic Fields*, edited by L. Neel (Elsevier, Amsterdam, 1979), pp. 127–139.
[23] J. Cahen-de Villardi, M. Clerc, P. Isnard, and J. M. Weulersse, J. Mol. Spectrosc. **84**, 319 (1980).
[24] A. Schultz and G. Marowsky, Appl. Phys. **B 29**, 255 (1982).
[25] W. F. Adolfson, R. G. Schlecht, and J. B. Morton, Appl. Phys. **14**, 49 (1977).
[26] E. R. Bernstein and G. R. Meredith, Chem. Phys. **24**, 289, 301, 311 (1977).
[27] The most populated rotational level, J_{max}, is calculated from

$$N_j = \epsilon(2J+1)\exp[-BJ(J+1)\,hc/kT],$$

where ϵ is the nuclear spin degeneracy.

$$\epsilon = 2A_1 + 10A_2 + 8E + 6F_1 + 6F_2;$$

here $A_1, A_2, \cdots$ are the *number* of $A_1, A_2, \cdots$ levels in the manifold. The common approximation

$$J_{max} \approx (kT/hcB)^{1/2} - 1/2$$

(which is valid for $\epsilon \propto 2J+1$ and thus only for *accidentally* spherical tops) gives $J_{max} = 61$ instead of 63 at 300 K.
[28] J. J. Katz and E. Rabinowitch, *The Chemistry of Uranium. Part I. The Element, Its Binary and Related Compounds* (McGraw-Hill, New York, 1951), Chap. 13. The vapor pressures quoted here for solid UF_6 were calculated from the Kirshenbaum equation [Katz and Rabinowitch, p. 407, Eq. (27)]. These are in good agreement with the more recent measurements of D. F. Smith, W. G. Schwab, and T. G. Burke [Appl. Opt. **2**, 1165 (1963)] down to 218 K; D. Meixner, A. Heintz, and R. N. Lichtenthaler [Ber. Bunsenges. Phys. Chem. **82**, 220 (1978)] down to 250 K; and Kim and Person (Ref. 33) for 160–220 K.
[29] D. N. Travis, J. C. McGurk, D. McKeown, and R. G. Denning, Chem. Phys. Lett. **45**, 287 (1977).

[30]G. S. Baronov, A. D. Britov, S. M. Karavaev, A. I. Karchevskii, L. N. Kurbatov, S. Yu. Kulikov, A. V. Merzlyakov, and S. D. Sivachenko, Izvest. Akad. Nauk SSSR, Ser. Fiz. **45**, 1500 (1981).
[31]G. S. Baronov, A. D. Britov, S. M. Karavaev, A. I. Karchevskii, S. Yu. Kulikov, A. V. Merzlyakov, S. D. Sivachenko, and Yu. I. Shcherbina, Kvant. Elekt. **8**, 1573 (1981); Sov. J. Quantum Electron. **11**, 947 (1981).
[32]K. C. Kim and H. Filip, Appl. Spectrosc. **39**, 167 (1985).
[33]K. C. Kim and W. B. Person, J. Chem. Phys. **74**, 171 (1981).
[34]B. J. Krohn and K. C. Kim, J. Chem. Phys. **77**, 1645 (1982).
[35]M. Takami, T. Oyama, T. Watanabe, S. Namba, and R. Nakane, Jpn. J. Appl. Phys. **23**, L88 (1984).
[36]A. H. Shapiro, *The Dynamics and Thermodynamics of Compressible Fluid Flow* (Ronald, New York, 1953), Vol. I, p. 83.
[37]H. W. Liepmann and A. Roshko, *Elements of Gasdynamics* (Wiley, New York, 1957), pp. 49–50.
[38]W. B. Olson, A. G. Maki, and W. J. Lafferty, J. Phys. Chem. Ref. Data **10**, 1065 (1981).
[39]K. Jolma, J. Kauppinen, and V. -M. Horneman, J. Mol. Spectrosc. **101**, 278 (1983).
[40]J. Moret-Bailly, Cahiers Phys. **15**, 237 (1961).
[41]J. Moret-Bailly, J. Mol. Spectrosc. **15**, 344 (1965).
[42]K. T. Hecht, J. Mol. Spectrosc. **5**, 355 (1960).
[43]E. B. Wilson, J. Chem. Phys. **3**, 276 (1935).
[44]C. D. Cantrell and H. W. Galbraith, J. Mol. Spectrosc. **58**, 158 (1975).
[45]A. J. Dorney and J. K. G. Watson, J. Mol. Spectrosc. **42**, 135 (1972).
[46]K. Fox, H. W. Galbraith, B. J. Krohn, and J. D. Louck, Phys. Rev. A **15**, 1363 (1977).
[47]W. G. Harter and C. W. Patterson, J. Chem. Phys. **66**, 4872 (1977).
[48]C. W. Patterson and W. G. Harter, J. Chem. Phys. **66**, 4886 (1977).
[49]H. W. Galbraith, C. W. Patterson, B. J. Krohn, and W. G. Harter, J. Mol. Spectrosc. **73**, 475 (1978).
[50]B. Bobin and K. Fox, J. Phys. (Paris) **34**, 571 (1973).
[51]J. Moret-Bailly, L. Gautier, and J. Montagutelli, J. Mol. Spectrosc. **15**, 355 (1965).
[52]B. J. Krohn, Los Alamos National Laboratory Report LA-6554-MS (Oct. 1976).
[53]R. S. McDowell, H. W. Galbraith, B. J. Krohn, C. D. Cantrell, and E. D. Hinkley, Opt. Commun. **17**, 178 (1976).
[54]M. Loëte, A. Clairon, A. Frichet, R. S. McDowell, H. W. Galbraith, J.-C. Hilico, J. Moret-Bailly, and L. Henry, C. R. Acad. Sci. (Paris) **285 B**, 175 (1977).
[55]Ch. J. Bordé, M. Ouhayoun, A. van Lerberghe, C. Salomon, S. Avrillier, C. D. Cantrell, and J. Bordé, in *Laser Spectroscopy IV*, edited by H. Walther and K. W. Rothe (Springer, Berlin, 1979), pp. 142–153.
[56]R. S. McDowell, M. J. Reisfeld, H. W. Galbraith, B. J. Krohn, H. Flicker, R. C. Kennedy, J. P. Aldridge, and N. G. Nereson, J. Mol. Spectrosc. **83**, 440 (1980).
[57]C. W. Patterson, R. S. McDowell, N. G. Nereson, B. J. Krohn, J. S. Wells, and F. R. Petersen, J. Mol. Spectrosc. **91**, 416 (1982).
[58]R. S. McDowell, M. J. Reisfeld, C. W. Patterson, B. J. Krohn, M. C. Vasquez, and G. A. Laguna, J. Chem. Phys. **77**, 4337 (1982).
[59]A. S. Pine, A. G. Maki, A. G. Robiette, B. J. Krohn, J. K. G. Watson, and Th. Urbanek, J. Am. Chem. Soc. **106**, 891 (1984).
[60]B. J. Krohn, J. Mol. Spectrosc. **73**, 462 (1978).
[61]B. J. Krohn and J. K. G. Watson (in preparation).
[62]K. C. Kim, W. B. Person, D. Seitz, and B. J. Krohn, J. Mol. Spectrosc. **76**, 322 (1979).
[63]E. G. Brock, B. J. Krohn, R. S. McDowell, C. W. Patterson, and D. F. Smith, J. Mol. Spectrosc. **76**, 301 (1979).
[64]R. S. McDowell, H. W. Galbraith, C. D. Cantrell, N. G. Nereson, and E. D. Hinkley, J. Mol. Spectrosc. **68**, 288 (1977).
[65]C. W. Patterson, B. J. Krohn, and A. S. Pine, J. Mol. Spectrosc. **88**, 133 (1981).
[66]C. W. Patterson and A. S. Pine, J. Mol. Spectrosc. **96**, 404 (1982).
[67]C. W. Patterson, R. S. McDowell, N. G. Nereson, R. F. Begley, H. W. Galbraith, and B. J. Krohn, J. Mol. Spectrosc. **80**, 71 (1980).
[68]H. M. Seip, Acta Chem. Scand. **19**, 1955 (1965).
[69]M. Kimura, V. Schomaker, D. W. Smith, and B. Weinstock, J. Chem. Phys. **48**, 4001 (1968).
[70]G. Herzberg, *Molecular Spectra and Molecular Structure. II. Infrared and Raman Spectra of Polyatomic Molecules* (Van Nostrand, Princeton, 1945), pp. 210f.
[71]R. S. McDowell, B.J. Krohn, H. Flicker, M. Vasquez, and J. L. Lyman (in preparation).
[72]J. Bron, Can. J. Chem. **54**, 160 (1976).
[73]J. Bron and R. Wallace, J. Chem. Soc. Faraday Trans. 2 **74**, 611 (1978).
[74]The FG-matrix treatment of octahedral XY_6 molecules has been discussed by many authors; for example, C. W. F. T. Pistorius, J. Chem. Phys. **29**, 1328 (1958); S. Abramowitz and I. W. Levin, *ibid.* **44**, 3353 (1966); and A. Fadini and S. Kemmler-Sack, J. Mol. Struct. **62**, 287 (1980). Our notation for the valence interaction force constants is also given in the footnote to Table IV of Ref. 14. Note the definition of F_{34} in Table VII: $F_{34} = 2(f_{r\alpha} - f''_{r\alpha})$ where the force constants are for the interactions between a U–F bond and a F–U–F angle containing ($f_{r\alpha}$) and excluding but coplanar with ($f''_{r\alpha}$) that bond. Some authors (including Pistorius, and Abramowitz and Levin) use a convention having the opposite sign, and this should be kept in mind when comparing values of F_{34} from different papers. The calculations employed the 1973 CODATA values for the physical constants, with atomic masses of 18.998 403 3, 235.043 925, and 238.050 786 amu for fluorine and the two uranium isotopes, respectively. All force constants are quoted in units of mdyn/Å (1 mdyn/Å = 100 N/m).
[75]J. C. Cummings, J. Mol. Spectrosc. **83**, 417 (1980).
[76]M. Takami and H. Kuze, J. Chem. Phys. **80**, 5994 (1984).
[77]R. S. McDowell, R. J. Sherman, L. B. Asprey, and R. C. Kennedy, J. Chem. Phys. **62**, 3974 (1975).
[78]M. Takami, J. Chem. Phys. **74**, 4276 (1981).
[79]R. S. McDowell, C. W. Patterson, and W. G. Harter, Los Alamos Science **3** (1), 38 (Winter/Spring 1982).
[80]L. Halonen and M. S. Child, J. Chem. Phys. **79**, 559 (1983).
[81]A. S. Pine and A. G. Robiette, J. Mol. Spectrosc. **80**, 388 (1980).
[82]A. G. Robiette, D.L. Gray, and F. W. Birss, Mol. Phys. **32**, 1591 (1976).
[83]R. S. McDowell, M.J. Reisfeld, N. G. Nereson, B. J. Krohn, and C. W. Patterson, J. Mol. Spectrosc. (in press).
[84]K. C. Kim, R. A. Briesmeister, G. M. Campbell, and W. B. Person, Chem. Phys. Lett. **104**, 79 (1984).